Master's Theses (2009 -)   Dissertations, Theses, and Professional
                                                                                      Projects

Investigation of Optimization Targets for Predictive Simulation of Human Gait with Model Predictive Control

Jessica Brianne Thayer
Marquette University

Follow this and additional works at: https://epublications.marquette.edu/theses_open

Part of the Engineering Commons

INVESTIGATION OF OPTIMIZATION TARGETS FOR
PREDICTIVE SIMULATION OF HUMAN GAIT
WITH MODEL PREDICTIVE CONTROL

by

Jessica B. Thayer, B.S.

A Thesis submitted to the Faculty of the Graduate School,
Marquette University,
in Partial Fulfillment of the Requirements for
the Degree of Master of Science

Milwaukee, Wisconsin

August 2020

ABSTRACT
INVESTIGATION OF OPTIMIZATION TARGETS FOR
PREDICTIVE SIMULATION OF HUMAN GAIT
WITH MODEL PREDICTIVE CONTROL

Jessica B. Thayer, B.S.

Marquette University, 2020

The design and development of gait-related treatments and devices is inhibited by an absence of predictive gait models. Understanding of human gait and what motivates walking patterns is still limited, despite walking being one of the most routine human activities. While a significant body of literature exists on gait modeling and optimization criteria to achieve simulated, normal gait, particularly with neuromuscular models, few studies have aimed to apply optimization targets which approximate metabolic cost to mechanical gait models. Even fewer have attempted this predictively, with no joint angle data specified *a priori*. The Sun model [31], [32] is one such mechanical framework which utilizes MPC to predict the dynamics of human walking. This thesis expands the Sun model [31], [32] to simulate a full gait cycle (CG) and investigates the application of new optimization targets within an existing Model Predictive Control (MPC) framework for predictive gait simulation developed by Sun [31], [32] .

The Sun model [31], [32] was previously limited to a half gait cycle (GC) which assumed bilateral symmetry and optimized only according to characteristic constraints such as step length and velocity of the center of mass (COM). In this thesis, the Sun framework and MPC control scheme were expanded to generate consecutive double support (DS), single support (SS), DS, and SS period simulations, which constitutes a full GC. The resulting GC simulation was not marked by GC events toe off (TO) and heel strike (HS), but did achieve continuity over the period which was not achieved by the Sun model [31], [32] . Additionally, new cost functions were developed consistent with existing literature which suggests that the Central Nervous System (CNS) uses a variety of energy-related targets in generating gait. This thesis demonstrates that the application of optimization targets which approximate metabolic costs is possible with the proposed MPC framework for a mechanical gait model, but that the performance of resulting simulations should not be evaluated until a full GC marked by TO and HS is achieved.

While a continuous full GC simulation was achieved, the failure of the model to reliably meet characteristic constraints, particularly in SS, prevents simulation of a GC marked by TO and HS. The work in this thesis points primarily to the failure of the optimization routine within the MPC framework to reliably find a solution that meets constraints as the cause of this problem. If the optimization problem can be classified, an appropriate solution algorithm could be chosen which could reliably find a solution for any given set of constraints and initial conditions (IC). Identifying an appropriate solution algorithm could make the MPC framework proposed a viable method of gait prediction and simulation.

This investigation provides researchers better understanding of the application of energy-based optimization in mechanical gait models and the current limitations of gait prediction and simulation. In addition, direction is given to the future work necessary to establish MPC as a viable control method for gait simulation.

ACKNOWLEDGMENTS

Jessica B. Thayer, B.S.

This research would not have been possible without the mentorship of Dr. Philip Voglewede. The best teacher I've had the pleasure of learning from (and teaching with), he gave me the direction, support, and motivation to make this project happen and the grace to pivot when the research didn't go according to plan. I would also like to thank Drs. Gerald Harris and Jacob Rammer for sharing their gait analysis and motion capture expertise and Dr. John Moore for his experience with numerical methods and optimization. Tom Current, CPO is also thanked for his clinical expertise and fabrication of AFOs for the study, without which we could not fully evaluate the work presented in this thesis.

Engineering is and always will be a team sport, and I'm eternally thankful for the small army of mentors and friends who've made Marquette University home. No amount of thanks can repay a fraction of what the faculty and staff at Marquette have invested in me. To Dr. Ropella, Kate Trevey, Andrea Gorman, and Julie Murphy, I'll forever be grateful for your challenging me to do better, dream bigger, and always making yourselves available to talk through the big decisions. To Eileen Baker, thank you for the numerous proofreadings and research discussions, and to Tom Ruopp, Joey Avila, and Dan Garcia, thanks for the companionship throughout the countless hours of work in E-Hall.

Finally, to my parents, thank you for letting me pick my most expensive school option six short years ago and helping me figure out how to make it work. My time at Marquette has changed me immeasurably, and I can never thank you enough for getting me here.

The Marquette University Department of Mechanical Engineering is gratefully acknowledged for its financial support of the author.

TABLE OF CONTENTS

LIST OF FIGURES

LIST OF ACRONYMS

Acronym	Meaning
AFO	Ankle Foot Orthosis
COM	Center of Mass
CMA	Center for Motion Analysis [1]
CNS	Central Nervous System
CPG	Central Pattern Generator
DOF	Degree of Freedom
DS	Double Support
GC	Gait Cycle
HAT	Head, Arms, and Torso
HS	Heel Strike
HZD	Hybrid Zero Dynamic
IC	Initial Conditions
KAD	Knee-Alignment Device
MCW	Medical College of Wisconsin
MIMO	Multiple Input Multiple Output
MOO	Multi-Objective Optimization
MPC	Model Predictive Control
MPIC	Model Predictive Impedance Control
OREC	Orthopedic Rehabilitation Engineering Center [2]
PID	Proportional, Integral, Derivative (Control)
P&O	Prosthetics and Orthotics
ROM	Range of Motion
SS	Single Support
TO	Toe Off
ZMP	Zero-Moment-Point

CHAPTER 1

INTRODUCTION

Walking is one of the most routine activities that humans do every day, both as a form of exercise and as a valuable aspect of independence and self-sufficiency. Ambulation in healthy individuals enables the performance of daily tasks and drastically improves quality of life, and therefore, if ambulation is impaired, longevity also decreases [14]. Positive effects of walking have also been seen in diseased populations, as walking has been shown to mediate the effects of diabetes, cancer, depression, and extend the lifespan of individuals with high blood pressure or struggling with obesity [14], [10]. While any regular exercise is beneficial to overall physical and mental health, walking in particular is a great, low-impact form of exercise throughout a person's lifetime [15].

Challenges to ambulation can arise due to loss of limb, as approximately 185,000 patients in the United States alone undergo a lower-limb amputation annually [43]. Of the nearly 2 million individuals in the US who have lost a limb, the leading cause of amputation is vascular disease such as diabetes (54%) followed closely by trauma (45%) [9], with numbers projected to increase. Adding to the already traumatic experience of amputation, the slow, trial-and-error process of fitting a prosthetic device can produce feelings of frustration and hopelessness in patients struggling to regain normalcy. Currently, the prosthetic fitting process is heavily reliant on experimentation, where the mechanical device itself can be modified based on prosthetist preference, then fabricated and fitted for patient use through an iterative process. On average, it takes approximately five months and multiple visits to a clinician from the time of amputation surgery for a patient to be comfortably fitted with a permanent prosthetic device [20].

1.1 Problem Statement

Though learning to walk is a natural part of human development, current understanding of human gait is limited, inhibiting the application and development of gait-related treatments and medical devices such as prosthetics and orthotics (P&O). Passive prostheses, without energy input, have been developed but fail to provide the forces necessary for complete desired mobility, particularly in the stance phase of gait. Alternatively, active prostheses use an actuator to input energy into the prosthesis and offer significant advantages over passive devices by providing power in the toe-off phase of gait to fully restore normal gait. Development of active prostheses,

however, is limited by gait models that lack predictive capabilities. Speed and efficiency in design iterations will continue to grow more necessary as lower limb prosthetic design becomes increasingly complex and the number of amputees grows.

A better understanding of human gait, both normal and pathological, is necessary to improve the development and fitting of P&O for amputees. **Improvement of the design and development of gait related treatments and devices requires gait models that allow for the *prediction* of normal and pathological gait** so that experimental gait analyses are not required. Thus, it is necessary that this prediction is computationally efficient and adaptable, requiring less time than standard gait testing methods. Primarily, an improved gait model would enable new gait related devices to be virtually tested on a patient-specific model of normal gait, allowing for quicker performance prediction, lower cost of development, and reduced risk of injury during subject testing.

1.2   Specific Aims

Using an existing gait model and control system proposed by Sun [31], [32] , this research improves the performance criteria used within the optimization framework to better model gait generation by the central nervous system (CNS).

The three aims of this thesis were as follows:

Aim 1: To expand the Sun model [31], [32] to predict a subject-specific gait cycle (GC).

Using the Sun framework [31], [32] and model predictive control scheme, a full GC will be generated with subject-specific anthropomorphic parameters. These subject-specific models will be used to examine the effects of new cost functions, and will be evaluated using clinical gait analysis tools following subject trials.

Aim 2: To develop cost functions consistent with existing literature to better mimic CNS control of the body during gait.

Literature suggests that the CNS uses a variety of energy-related targets in generating gait [3], [7], [40], and this work aims to incorporate cost functions that minimize measures of metabolic energy expenditure using the original Sun model targets to most closely predict and simulate normal gait. The first cost functions explored will aim to minimize mechanical approximations of metabolic cost or fatigue and the Sun model's original optimization targets. These additional measures include external work on the center of mass

(COM) *[7], the summation of the joint torques [40], and muscle fatigue [3].*

Aim 3: To evaluate controller performance using clinical gait analysis measures in prediction of both normal and abnormal human gait.

Resulting optimization schemes will be used to predict both normal and rigid-ankle pathological gait. Joint angle profiles from this study will be compared to 3D motion capture kinematic data of subjects walking both unhindered (normal case) and with a rigid AFO (pathological) to inhibit ankle flexion. Additionally, the joint angle profiles from these simulations will also be compared with a normal ambulator database [2] and the Sun model.

The gait simulation framework proposed by the author is an expansion of the Sun model [31], which is unique in its predictive approach. This investigation will provide researchers better understanding of the application of energy-based optimization in mechanical gait models and the current limitations of gait prediction and simulation. In addition, direction is given to the future work necessary to establish MPC as a viable control method for gait simulation.

CHAPTER 2

LITERATURE REVIEW

Gait research can be divided into two categories: gait analysis and gait simulation. Gait analysis allows for definition and identification of pathological gait as deviant from normal. Current gait analysis practices allow for three-dimensional motion tracking, which eliminates the limitations of two-dimensional observational analysis, and have been used to understand factors that influence normal walking patterns. However, in observing abnormality in gait analysis, it is difficult to differentiate between the *mechanical* influence of the body's physical limitations or the *motivational* influence of the CNS that generates human gait.

Alternatively, gait simulation provides insight into the effect of both mechanics and motivation in human walking. Gait simulations across existing literature vary greatly in complexity and goal but are differentiable both by gait model and simulation method. Gait models represent the physical limitations and dynamics of human walking with mathematical approximations, i.e., the *mechanics* of human movement. The simulation methods used to manipulate these gait models also vary, but represent the *motivation* of human movement. Evaluation tools for these gait simulations can be derived from kinematic and kinetic gait analysis to describe simulation accuracy.

Section 2.1 describes pertinent clinical observations of human gait. Sections 2.2 and 2.3 detail the current state of gait analysis and simulation methods, respectively. Finally, Section 2.4.1 discusses the variety of literature pertaining to optimization targets for gait simulation.

2.1 Human Gait

To create a predictive model of human gait, an understanding of normal ambulation is necessary. Human gait is a cyclic limb pattern to advance the body and consists of two dynamically distinct *phases*: stance and swing (Figure 2.1), which describe the motion of each limb individually. Stance phase is characterized by the foot being in contact with the floor and begins with initial contact, or heel strike for normal ambulators. Swing phase begins with toe-off and consists of a free-swinging pendulum to advance the limb. These phases together make up one gait cycle (GC) in time and one stride (or two steps) in distance. The GC is also characterized by eight distinct muscle activation *events*: initial contact, loading response, mid-stance, terminal stance, pre-swing, initial swing, and terminal swing [28]. Position in the gait cycle can be
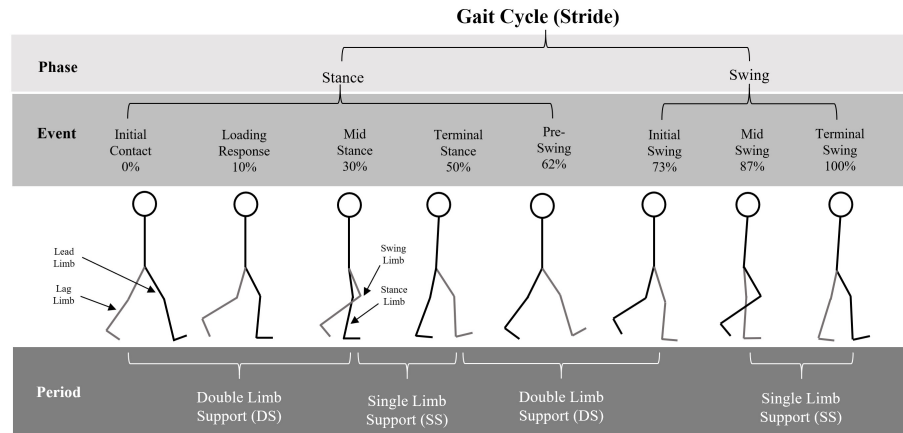
Figure 2.1: Gait cycle phases and events [28].

described by these event markers, time, or percent GC (%GC), shown in Figure 2.1.

Each step is also subdivided into two *periods*, which are also dynamically distinct: double limb support (DS), and single limb support (SS). These periods describe the motion of both limbs, and are the major subdivisions used for the prediction and simulation of gait in this study. Between these periods, the mechanical energy of the body is exchanged between kinetic and potential energy during forward translation of the COM during double support, and the upward shift of the COM as the head-arms-torso (HAT) rocks over the stance leg during single support, respectively [19], [27]. These periods of energy expenditures become important in understanding the GC. Minimizing energy expenditure is thought to be a primary target of gait generation, but the kinetic-potential energy exchange is incomplete and must be captured by an optimization routine to accurately predict gait.

Sections 2.1.1 and 2.1.2 highlight important characteristics and other relevant clinical observations of these periods, many of which contribute to or are ways to minimize the energy expenditure of the GC.

2.1.1 Double Limb Support Period

During DS, the weight of the HAT shifts from the lag limb to the lead limb in preparation for SS. DS begins with heel strike of the lead foot and weight acceptance onto the lead limb, and continues until the lag limb pushes off the ground at toe-off (TO). Though less total external work is required for stiff-legged weight acceptance, normal gait patterns prioritize minimizing ground contact forces and reducing the vertical translation of the COM by bending the leg at heel

strike [19], [3].

During this period, external work is needed to shift the COM forward. Cavagna et al. demonstrated that up to nearly 7 km/hr walking speed, COM displacement during DS is constant for an individual [8]. Given the limited range of the DS period, studies have proposed that the muscle action during DS solely establishes an appropriate set of initial conditions for the SS period [26].

2.1.2 Single Support Period

SS advances the swing leg to complete a step. This forward progression of the leg is measured as step length and is frequently used as a measure of gait stability [40]. The change in potential energy as the COM shifts up and over the stance leg is the primary driver of metabolic cost in this period, though the pendulum action of the swing leg offsets energy expenditure [8]. However, normal ambulators seemingly aim to minimize this expenditure by shortening the "virtual stance limb," which is the distance from the COM to the foot's point of contact with the ground [19].

SS can very nearly be modeled as an inverted pendulum [8], but the simplified model does not capture the metabolic cost perfectly [27]. Because there is minimal muscle activation during SS, the "initial conditions," or the transition from DS to SS, is significant in the successful completion of a step [26] [13].

2.2 Gait Analysis

Gait analysis is the act of making biomechanical interpretations of observed or collected data to understand why a person walks the way they do. A variety of gait parameters have been adopted as part of clinical gait analysis, including, but not limited to: stride length, step length, cadence, duration of SS, walking speed, and percent of cycle for specific gait events [6]. In addition to these temporal parameters, kinematic data can also be used to identify "features" of gait, where it deviates from normal. A common plot convention used in gait analysis (see Figure 2.2) will be used in this work to highlight features of the simulated gait and make comparisons with kinematic data from subject testing.

This plot convention highlights the range of normal gait kinematic data in the sagittal, coronal, and transverse planes (left to right) for the particular database used (shown as green bands) of each lower limb segment, proximal to distal (top to bottom). The right leg (red lines)
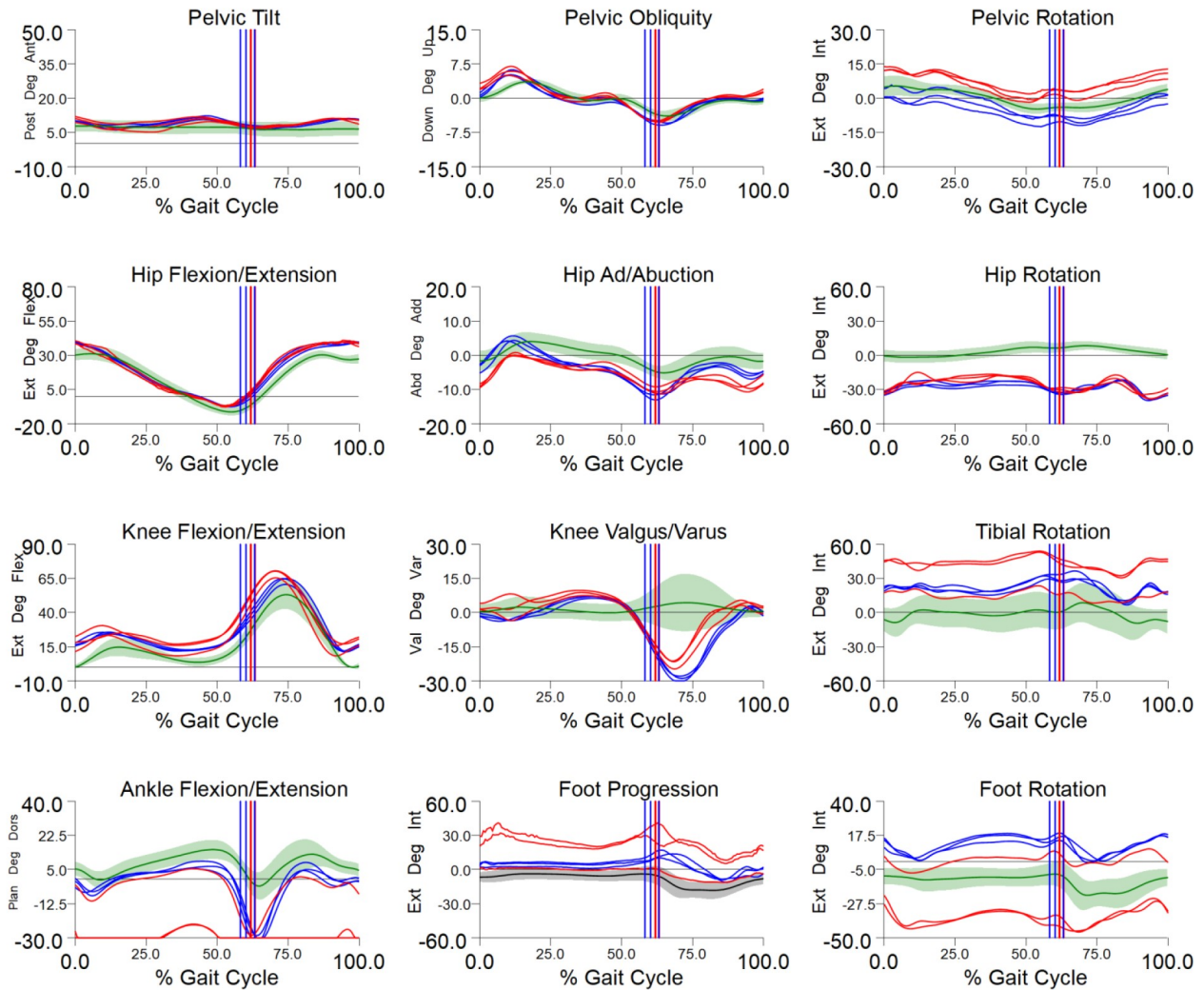
Figure 2.2: Plot Convention for gait analysis kinematic data [2]. The data presented is an example of results collected outside of this thesis and includes outliers in the right limb data.

and left leg (blue lines) joint kinematic data acquired through a single or series of walking trials is superimposed on the normal bands to allow for comparison. The red and blue vertical lines identify the %GC where toe-off occurs. The angle of the distal segment is defined relative to an extension of the line along the axis of the proximal segment, beginning at the pelvis and measured from anatomical neutral. For each joint, flexion (dorsiflexion at the ankle) is assumed positive, and extension (plantarflexion) is negative.

An evaluation of gait simulated by the improved model will be made consistent with clinical gait analysis practices. The specific measures to be compared are sagittal plane kinematic data and step length.
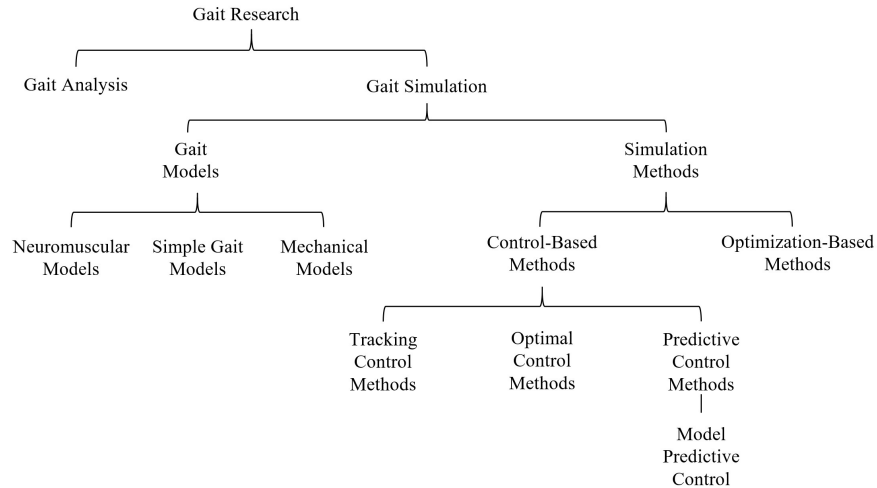
Figure 2.3: Classification of current human gait research.

A tremendous amount of literature has been published about gait analysis and normal gait [39] [28]. Only a brief summary has been provided in this thesis to provide important features relevant to the prediction of gait and observations necessary for evaluation of gait models.

2.3 Gait Simulation

A number of gait simulations exist of varying complexity and can be categorized as biomechanics gait analysis or biped robotics research. These simulations vary in complexity of the gait model and type of simulation method. Figure 2.3 shows the divisions of existing gait research.

2.3.1 Gait Models

Gait models across literature vary greatly depending on modeling intent. On one end of the complexity spectrum these models represent a portion of the gait cycle with a simplistic mechanical approximation such as the inverted pendulum model. At the other extreme are high-fidelity neuromuscular models used as objects for computationally intensive optimization schemes.

Biomechanics Gait Models

Biomechanics gait models are typically neuromuscular models, meaning that muscle activation is modeled and used as actuation for the rigid body segments and joints. Gait has been

successfully simulated through such optimization methods. There exists significant evidence of central pattern generators (CPGs) for human locomotion, and Van der Noot et al. were able to incorporate CPGs in the control scheme for a neuromuscular model [34]. Alternatively, Anderson and Pandy developed a 23 degree-of-freedom (DOF) model actuated by fifty-four muscle groups and optimized a gait cycle muscle excitation pattern according to metabolic cost per unit distance traveled [4]. Because interest in such biomechanics optimizations have grown, the literature suggesting novel methods such as simulated parallel annealing [16] and residual elimination algorithms [29] have been proposed as less computationally intensive alternatives to the optimization problem.

Currently, processes for optimization of walking pattern parameters for biomechanics gait models are computationally intense and thus do not respond and adjust in real-time like the control of the central nervous system (CNS). High-fidelity biomechanics gait models are far too complex for real-time gait control.

Simplified Gait Models

The simplest models within biped robotics research include the inverted pendulum, the passive dynamic walker, and the Zero-Moment-Point method [40]. Using a concentrated body mass at the center of gravity and a planar inverted pendulum as a massless leg with variable length the inverted pendulum model can be used as a gait model. The passive dynamic walker model demonstrates that a biped model can walk down a ramp purely driven by gravity as the legs swing naturally like a pendulum [40]. This model was translated to the horizontal plane as well. The inverted pendulum and passive dynamic walker models are too simple to adequately model gait because they lack all lower extremity joints, but these models can still be used to generate or optimize robotic gait [37]. The zero-moment-point (ZMP) method generates gait by ensuring the stability of the body by following a pre-defined set of ZMP positions, where the resultant moments of active forces are zero [40]. Dynamics equations are used only to calculate these ZMP positions and not the entire trajectory. Variations of ZMP models have been used to control gait of several different biped robots with varying DOF from 7 to 26 [11], [42]. While computationally efficient, these simplified methods can manage real-time control, but as stability is not the primary human criteria for walking, they cannot effectively model the CNS.

Mechanical Gait Models

The majority of models without musculature can be described as "mechanical" models, and are designed to represent the dynamics of the human body during gait with simplified actuation. Usually these models consist of rigid links connected by revolute joints with a variety of complexity and ground reaction force models [7], [25], [30]. Mechanical models allow for evaluation of control schemes and optimization targets without the computational intensity of dynamic simulation of large DOF neuromuscular systems.

Despite being smaller DOF systems, mechanical gait models can offer relatively high levels of fidelity. The Sun Model [31], [32], the basis for this thesis, is a mechanical model, as are most models used with control-based simulation methods (Section 2.3.2).

2.3.2 Simulation Methods

Simulation methods used to manipulate gait models also vary in scope and complexity. Each simulation method can be used with any of the previously discussed gait models, though some applications are inherently more practical than others.

Optimization Based Methods

Optimization based methods focus on determining what criteria the CNS uses to generate gait and aim to optimize a trajectory to meet these criteria [40]. Many biomechanics gait simulations use optimization methods to identify a muscle activation pattern to achieve gait with low metabolic cost or muscle fatigue [4], [16]. In biped robotics research, the performance measures most commonly used are: dynamic effort, mechanical energy, metabolic energy, jerk, and stability [40]. By combining these objectives, the control of the CNS can be modeled with large DOF and have been successful in simulating gait. However, these methods are computationally-intensive and require experimental data, so they are not completely predictive, but give insight about CNS optimization targets.

Control Based Methods

Control based methods prove better suited to gait simulation and are widely used for both biomechanics and robotic gait simulations. Traditional PID control is insufficient for this study as it is reactionary, instead of predictive. However, a control-based method, given the right controller, can be robust, flexible, and handle environmental disturbances. Literature on

control-based methods for gait simulation is extensive, and control based gait simulation can be achieved using a variety of controllers. Katic and Vukobratovic [18] reviewed neural networks, fuzzy logic, genetic algorithms, and hybrid control algorithms for gait simulation. Several control based methods are reviewed in this section.

Hybrid Zero Dynamic (HZD) control-based models capture limited features of gait but allow rapid optimization [40]. Westerverlt et al. [38] used a hybrid-zero-dynamics feedback control method for planar biped gait, and Azevedo et al. [5] proposed a nonlinear predictive controller which calculated trajectories by minimizing an objective function. These methods successfully simulate gait, though not entirely predictively.

Control-based methods are also often used within optimization methods to predict necessary muscle forces for the optimized trajectories. There are three main categories of control-based methods:

Tracking Control Methods. Tracking control methods begin with a desired motion trajectory and calculate the proper torque inputs to follow that motion [40]. These methods, therefore, are not appropriate for this study, which aims to predict human gait without a priori joint trajectories.

Optimal Control Methods. A subset of control-based methods is optimal control methods, where the controller minimizes a cost function to direct the model from initial to final state [40]. These methods are similar to the optimization methods for gait simulation, where continuous torque inputs are the unknowns for the duration of the optimization period [40]. However, information about the initial and final states is still required, so the simulation cannot be entirely predictive.

Predictive Control Methods and Model Predictive Control. Predictive control methods make up the final sub-division of control-based methods and utilize iterative, finite horizon optimizations of the motion [40]. Martin and Schmiedeler have incorporated hybrid zero dynamics control into a predictive model of gait with a modified foot model to allow for the phase variable calculation required for HZD [22]. Another predictive control method is model predictive control, or MPC, used in this thesis. MPC is an iterative optimization of the motion that optimizes for the entire gait cycle, as opposed to optimal control methods, which commonly minimize the cost function only once. Only initial joint position information is required.
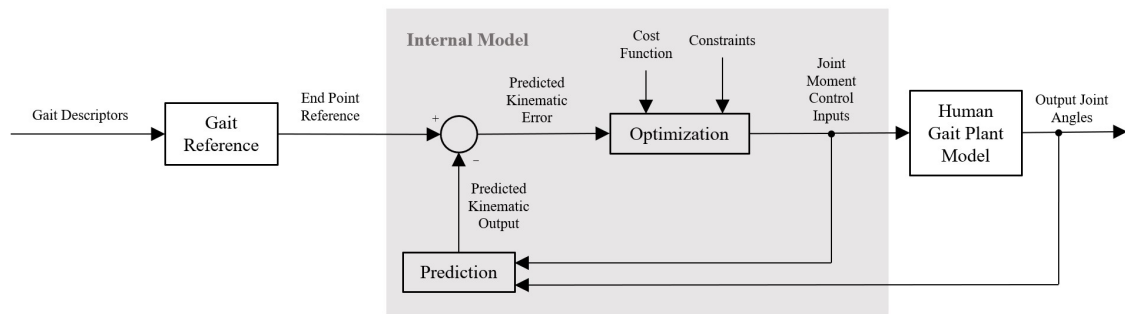
Figure 2.4: Block diagram of MPC as applied to human gait prediction.

2.3.3 Model Predictive Control for Gait Simulation

A general block diagram for MPC applied to gait can be seen in Figure 2.4. Van der Kooij et al. [33] were able to achieve repeated gait simulation by using MPC to control a 7-link, 8-DOF model by optimizing step time, step length, and the velocity of the center of mass at push-off, with prescribed end-states. Since end positions between phases of gait are specified [12], van der Kooij's work is not entirely predictive and could be classified as an optimal control method. However, this approach presents MPC as a viable control method for gait simulation and was unique in that most robotic field gait simulation uses dynamic effort and metabolic energy usage [33].

Minimization of mechanical energy expenditure was the main cost function of a similar MPC proposal by Ren et al. [30], which used an inverse dynamic formulation rather than a forward dynamic model. A single cycle was generated for another 7-link model with walking velocity, cycle period, and double stance phase duration as the predictive control references. Karimian et al. [17] used model predictive impedance control (MPIC) to control a 3D 5-segment gait model, which was able to climb and descend stairs. The cost function was energy consumption, vertical body orientation, and center of mass forward velocity. Each of these projects have shown MPC as an effective controller representative of the CNS because of its flexibility. This thesis aims to explore additional combinations of control objectives.

MPC is a good approach for control of a human gait model because of its formulation and predictive approach. It is a state-space control method that works well with multiple input, multiple output (MIMO) systems. The simple MPC schematic shown in Figure 2.4 demonstrates

the predictive aspect of the MPC control scheme. The control input to the gait dynamics model is optimized according to the error between the target kinematic reference and the predicted kinematic output to the end of the gait cycle. This control output is then run for a specified time before the process is repeated.

Though MPC is promising as a control scheme for prediction of human walking patterns due to it's predictive capabilities, it is an optimal control method, meaning it is heavily dependent on successful optimization within the control framework. This iterative optimization can be challenging with nonlinear, high-DOF systems. A detailed description of MPC is given in Section 3.2.

The Sun Model

The Sun model [31], [32] proposed an improved MPC framework with a seven-link, nine-DOF human gait plant model, and provides the basis for this thesis. The Sun model [31], [32] uses a control system that is primarily MPC with secondary classical PID feedback controllers to mimic the CNS. The MPC method allows for constraints such as joint torque and range of motion limits to direct simulation of gait without any prior knowledge of gait or joint trajectories. This MPC method meets all necessary requirements for simulating the CNS—it is robust and flexible, can respond to disturbances, and though computationally intensive, a solution can be reached within reasonable time.

The Sun model [31] employs only endpoint MPC, meaning that the control algorithm compares only the final state to a target. While certain literature confirms this hypothesis and demonstrates that gait can be mostly described as an inverted pendulum in swing and a consistent HAT progression in stance [35], other literature suggests that the finer details of gait are controlled continuously to find the most efficient gait cycle [25].

The framework adopted from the Sun model [31], [32] will be further discussed in Chapter 3. The Sun model, like all MPC gait simulations, utilizes an optimization routine, as shown in Figure 2.4.

2.4   Cost Functions and Human Gait Optimization Criteria

The cost function, J, [36] is central to optimization within many gait simulation methods (including MPC and the Sun Model [31], [32]) and this thesis's work to improve the controller objective function, given by,

$$J(x(0), u) = \frac{1}{2} \sum_{k=N_0}^{N-1} [x(k)^T Q x(k) + u(k)^T R u(k)] + x(N)^T Q_f x(N), \qquad (2.1)$$

where N_0 is the current time, N is the final time step, Q is the weighting matrix for predicted

states, R is the weighting matrix from control inputs, and Q_f is the weighting matrix for the final

predicted states. Generally, the predicted future outputs (states), $x(k)$ with k as the current time

step, should be as close as possible to the reference from the cost function, J, while control effort,

$u(k)$, is minimized [31], [36]. The first term in this objective function is Stage Cost, the second is

Control Input Cost, and the last is Terminal Cost. By tuning Q, R, and Q_f, the importance of these

costs can be adjusted so that certain costs are enforced more strictly than others. The cost function

could consist of only one objective or a combination of varied objectives.

2.4.1   Optimization Targets

Optimization targets describe these individual objectives that make up the cost function,

and may consist of different types of costs (i.e., stage, control input, and terminal). Gait simulation

by control-based methods, described in prior sections, require optimization according to a cost

function, independent of whether the optimization is a tracking problem or a prediction. In gait

simulation, the cost functions usually consist of one or multiple optimization targets which are

approximations of measurable, physical quantities such as metabolic energy expenditure or step

length. Sun hypothesized that the CNS only controls a limited number of gait-descriptive

parameters in between the transitions of stance to swing and swing to stance [31]. Thus, the Sun

optimization targets were dominated by terminal cost, effective at the end of period simulations.

However, many studies have aimed to understand the priorities of the CNS in gait

generation [3], [4], [7], [19], [40]. Generally, it is concluded that the CNS is likely to prioritize

minimizing dynamic effort (the integral of the squares of all joint torques over time), muscle

fatigue, mechanical energy consumption, metabolic energy consumption, or maximizing

stability [40], in addition to achieving a specified step length and constant COM progression.

Dynamic effort and mechanical energy cost dominate performance measures used in

robotic gait simulation, while metabolic cost is primarily used in biomechanical gait analysis,

which uses detailed neuromuscular models. The Sun model optimizes joint angle trajectories to

meet a desired step length during single support stage of gait and target center of mass (COM)

velocity during the double support stage [31]. In reality, human gait is likely governed by a

combination of performance measures and optimization targets, and thus multi-objective optimization (MOO) methods may be required.

Metabolic Energy and Mechanical Approximations

Though mechanical approximations may be required because of the model used, a variety of studies demonstrate that metabolic energy savings is the primary optimization target in normal gait [25], primarily because muscles cannot be assumed to do work with constant efficiency. Mechanical work and dynamic effort can in theory predict metabolic energy expenditure when musculature is not included in a gait model. Burdett et al. [7] demonstrated that estimates of work done on body segments, an estimate of work done on the COM, or dynamic effort may be valid alternative optimization targets.

Effort and Fatigue

Energy-related optimization targets such as mechanical and metabolic energy approximations, discussed above, can be organized into effort and fatigue categories as proposed by Ackermann and Van den Bogert [3], who examined functions of weighted muscle activation patterns during optimization of gait cycle joint trajectories. Optimization targets that minimize muscle activation, weighted evenly or by volume, can be considered effort optimization targets. These functions result in reasonable gait characterized by straight-knee weight acceptance patterns [3]. A similar straight-legged weight acceptance pattern was oberved by Martin and Schmiedeler who predicted simplified patient-specific gait patterns by minimizing dynamic effort [22]. Fatigue optimization targets on the other hand minimize higher powers of muscle activation, penalizing over-exertion of individual muscle groups. These optimization targets achieve a bent-knee weight acceptance phase [3], which is consistent with normal human gait. This difference points to endurance or fatigue-avoidance as a viable optimization target in the prediction of human gait.

This thesis considers the use of mechanical approximation of metabolic cost and endurance measures for optimization in the prediction of human gait. The application of these optimization targets to the model framework is discussed in Section A.1.

CHAPTER 3

SIMULATION FRAMEWORK

The gait simulation framework used in this thesis is an expansion of the Sun model [31]. The Sun model consists of a seven-link, nine-DOF, forward dynamic human gait model as the plant, and a control system that is primarily Model Predictive Control (MPC) with secondary classical feedback control (PID), which together mimic the CNS [31]. This control method allows for constraints such as joint torque limits, range of motion limits, etc., to direct the simulation of gait without any prior knowledge of gait or joint trajectories. The gait simulation framework includes two plant models, two internal models, an objective function for each period (SS and DS) of gait, and a common optimization framework for both phases.

This chapter is dedicated to explaining each of these components within the framework (i.e., plant models, internal models, etc.) and the work adopted from the Sun model [31] in order to clearly delineate the new work completed and the limits of the framework. Sections 3.1 - 3.2 describe the MPC system created in the Sun model as applied in this thesis, which provides the framework for this thesis's objectives. Finally, Section A.1 details the optimization criteria used by Sun and the means by which these optimization criteria can be changed in addition to the modifications to the simulation framework made in this thesis.

3.1 The Plant Model

A seven-link, nine-DOF model of a human was developed [31], [32] and validated by open loop simulation with published joint torque data [39], shown in Figure 3.1. Movement is constrained to the sagittal plane, and the seven segments are the foot, shank, and thigh for each leg and a rigid mass representative of the head, arms, and torso (HAT). The model does not include a pelvis segment, which is instead modeled by an axis. Joint angles are measured as the position of the distal segment relative to an axis that extends from the proximal segment, relative to anatomical neutral. Hip angles are measured from an axis extending from the bottom of the HAT, which can result in a 5-degree extension shift because of the pelvis's average 5-degree anterior tilt during normal gait.

Each joint is an actuated, revolute joint with both passive and active actuation elements. Passive joint actuation consists of an internal passive rotational spring, *K*, and damper, *B*, used to model the limits and viscous damping, with spring and damping coefficients increasing
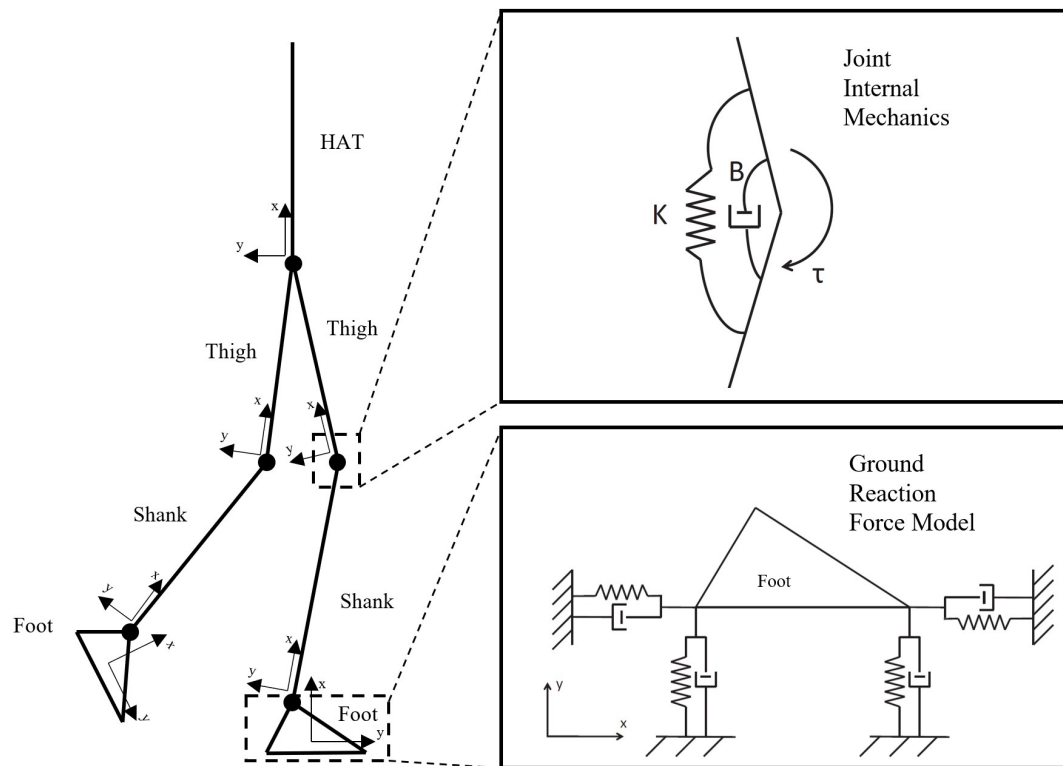
Figure 3.1: Human gait plant model.

exponentially as the joint moves outside a normal range of motion, with a mechanical stop at the absolute limits. Though there is no anatomy analogous to this internal spring, the springs function as passive feedback systems and stabilize the dynamics of gait, which is otherwise an inherently unstable process. An additional "hard stop" prevents the joints from over-extension, but is only activated when the joint position exceeds the joint limits. These internal mechanical parameters from the Sun model were optimized for each individual subject, which limits the generality of the model. For this thesis, internal mechanical parameters were not re-optimized for each subject, which does not affect the fidelity of the plant model.

Internal torques, τ, are also applied directly at the joint and represent the muscle activity surrounding the joint, and these internal torques, combined with the torques from the internal spring and damper cause the relative movement between the joints. The internal torques are controlled by PID or MPC as detailed throughout the rest of this chapter. When controlled by MPC, the internal torques consist of a two active components: a polynomial fit of a baseline

torque trajectory paired with an MPC control trajectory parameterized by a Laguerre function formulation. The MPC control trajectory and Laguerre function formulation are discussed in greater detail in Section A.1 and Appendix A. The baseline torque trajectory, or base polynomial, is fitted to Winter's published data [39] or subject-specific kinetic data from gait testing. The latter is not preferable, as it reduces the generality and predictiveness of the model by requiring gait analysis protocols of subjects, but can be used if an acceptable solution cannot be reached with Winter's data. Thus, there are five components of MPC joint actuation: linear passive springs and dampers, non-linear springs and dampers for joint limits, a mechanical hard stop, a baseline torque polynomial trajectory, and a Laguerre function formulation of the MPC control trajectory.

Ground reaction forces are modeled as a vertical and horizontal spring-damper pair at both the toe and heel, which act conditionally when the foot is in contact with the ground. These pairs model the stiffness, shock absorption, and energy dissipation between the foot and the ground.

Anthropometric parameters consist of segment lengths, masses, moments of inertia, and positions of the segments' COMs. These anthropometric parameter values can be measured during human subject testing or calculated using equations from Winter [39]. The parameterization of the models used in this simulation framework is discussed in Section 3.4.

Separate plants exist for both the SS and DS periods of gait because each phase is dynamically distinct. Note that the kinematic and kinetic parameters remain constant between the periods, but SS is an open kinematic chain, and DS is a closed kinematic chain. Simscape Multibody was used to create gait plant models which can be controlled by MATLAB (Figures 3.2, 3.3). This Simscape model is a graphical representation of the virtual human model and reproduces natural motion which can be used in prediction of gait.

3.2   The Control Framework

MPC (introduced in Section 2.3.2) was implemented in the Sun model to simulate the control of the CNS in walking [31], [32]. The MPC control scheme is shown in Figure 3.4 and is applied to the Sun Model and this thesis as follows:

1. Given model anthropometry at a sampling instant, k, the current states of the plant are $\mathbf{x}_k$. The future control trajectory is denoted $\Delta\mathbf{u}_k, \Delta\mathbf{u}_{k+1}, \ldots, \Delta\mathbf{u}_{k+N_C-1}$, where N_C is the *control horizon* which dictates the number of instances of future control input [36].
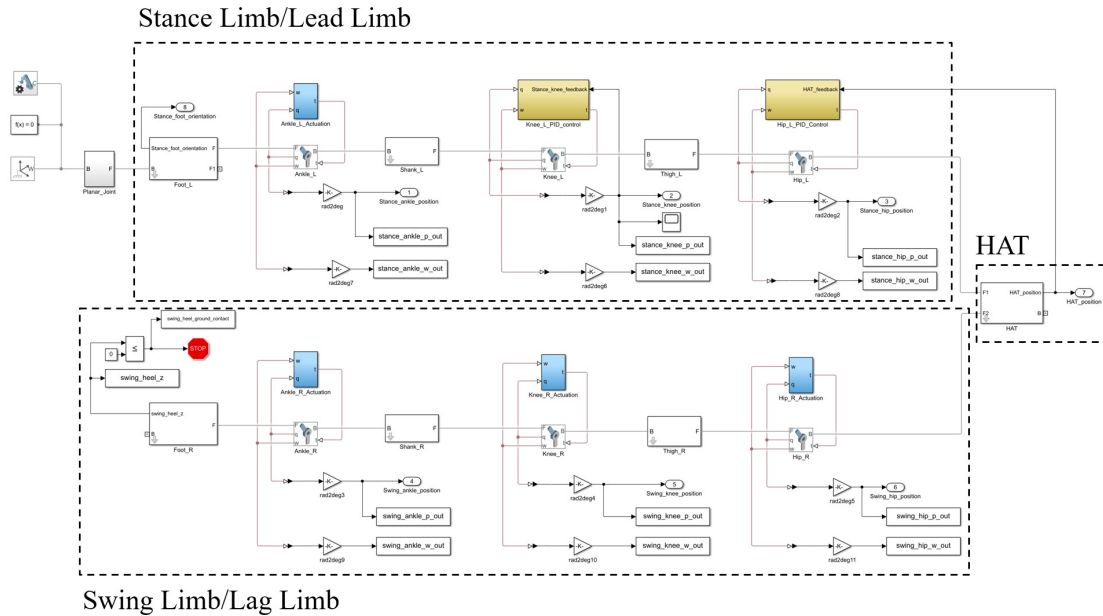
Figure 3.2: Simscape Multibody graphical representation of the plant model.

2. With the current states and future control trajectory, the future state variables for N_P number of samples are predicted using an *internal model*, where N_P is the *prediction horizon*. This prediction horizon is the length of the period of gait being predicted and thus, the length of the optimization window. The internal model is a simplified version of the plant and a state-space representation of the forward dynamics of human gait. Because of the discrete, state-space representation, the future predicted states can be written as a function of variable future control inputs. This process is shown as the "Prediction" block in Figure 3.4.

3. For given gait descriptors (i.e., step length, COM velocity, or approximate metabolic cost) as a reference set-point signal, the future control inputs are optimized to minimize the error between the internal model states and the set-point signal. This process is essentially the minimization of a cost function subject to constraints, using a gradient quadratic programming solution method in this framework. This process is the "Optimization" block in Figure 3.4.

4. After completing the optimization, the first time step, or *control window*, of the optimized control input are applied to the plant model, and the prediction-optimization process repeats until the end of the prediction horizon is reached. This simulation is shown as the "Plant" block in Figure 3.4.
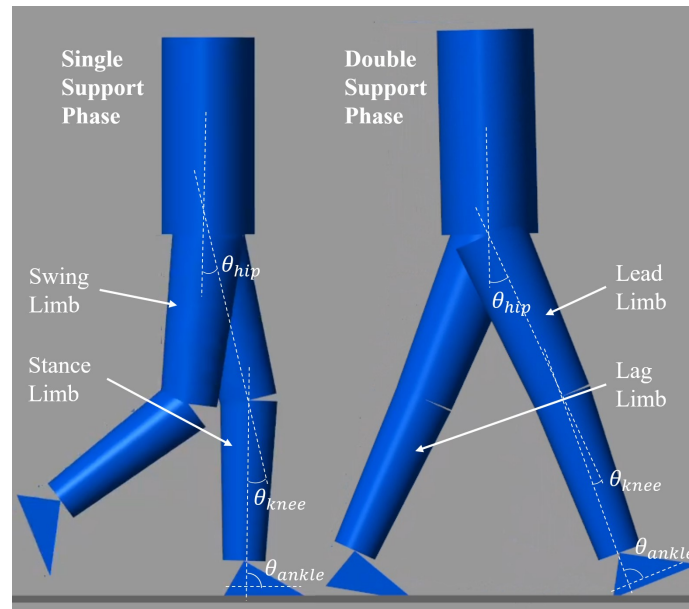
Figure 3.3: Simscape Multibody simulation of the plant model.
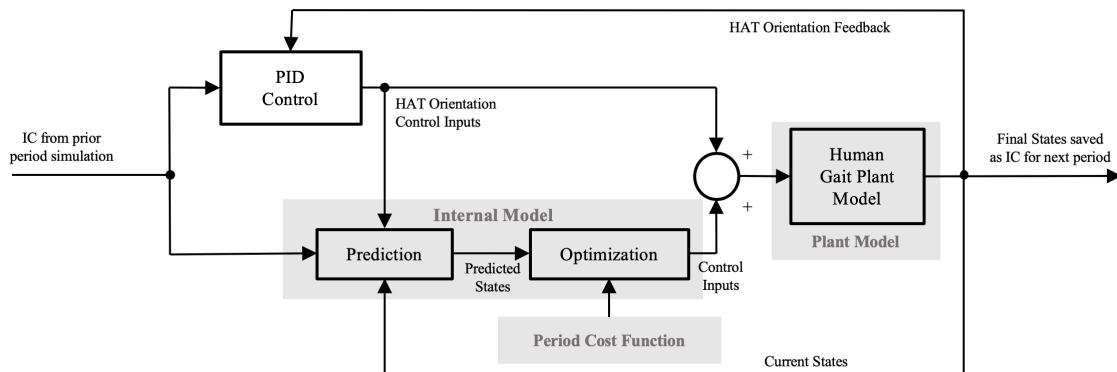
Figure 3.4: Overall simulation framework for prediction of one of four periods within the GC. This process repeats for DS, SS, DS, and SS period simulations.

This method is called "receding horizon control" because the prediction and control horizons shrink with each iteration. This MPC framework is applied to each period of gait in succession. The GC simulation developed in this thesis is marked left heel strike (LHS) to left heel strike and consists of two consecutive DS and SS simulation pairs.
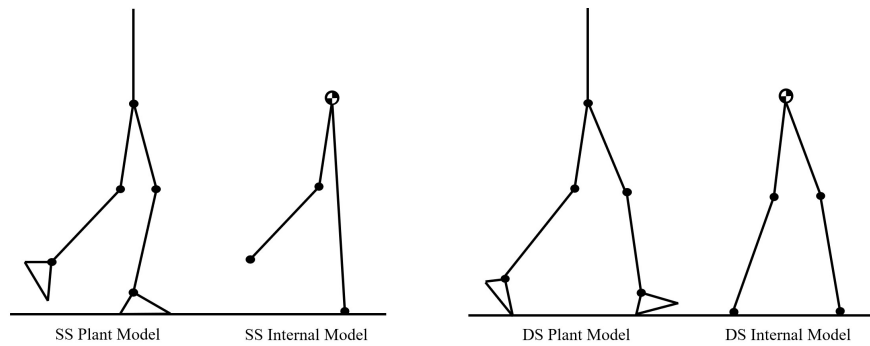
Figure 3.5: Simplified internal models for prediction.

Table 3.1: Joint control for SS and DS periods.

Period	Controller	Joint Angle
SS	MPC	stance ankle, swing ankle, swing knee, swing hip
	PID	stance knee, stance hip
DS	MPC	stance ankle, stance knee, swing ankle, swing knee
	PID	stance hip, swing hip

3.2.1   The Internal Models

Simplified models are used to reduce the computational intensity of the optimization. Shown in Figure 3.5, internal models for SS and DS were created and are used for prediction within the MPC algorithm (shown as "Prediction" block in Figure 3.4).

Both SS and DS internal models are used to optimize joint moments of four joints, and the remaining two are controlled by auxiliary PID controllers to reduce the computational load (Table 3.1). These moments are then saved to be applied to the full plant model. Joint actuators in the internal models are the same five-component joint moments as the plant. No changes were made to the Sun internal models for this thesis.

3.2.2   The Prediction and Control Horizons

MPC uses the simplified internal models to control joint angle trajectories of the plant by optimizing joint moments to a cost function. The trajectories from the internal models are predicted only in terms of the current state information and future control movement. The joint moments (i.e., control inputs) are calculated for the length of the control horizon, with states

determined by the current plant information and the predicted trajectories. These control inputs are then applied to the plant for one time-step, or the length of the *control window*. The same prediction and optimization are repeated for the next time-step, but then for shorter horizons. The process is repeated until the system reaches the final state. In this way, the trajectories of the system are predicted *and* optimized for a prescribed time period.

The Sun Model uses equal prediction and control horizons that recede as the optimization nears the end of the gait period.

3.3   Model Optimization Criteria and Constraints

The rest of this chapter details optimization criteria and the form of the cost function, $J(\mathbf{p})$, where $\mathbf{p}$ is an array of the control inputs for each MPC-controlled joint, for the simulation framework. The simulation framework proposed utilizes both optimization *targets* and *constraints* to predict walking patterns. Optimization targets are components of the cost function which the framework aims to minimize in its prediction of control inputs. The optimization constraints may be *physical* constraints such as joint limits, or *characteristic* constraints, which could dictate the end state of a simulation period.

The information about optimization targets is contained in an objective function for each phase (Section 2.4). MPC requires finding of an optimal control input solution which meets target gait descriptors, such as step length or walking speed, repeatedly. The optimization scheme by which this solution is found is flexible. This simulation framework uses a nonlinear programming solver within MATLAB to find the minimum of a constrained, nonlinear, multivariable function:

Minimize: $J(\mathbf{p})$

Subject to: $\mathbf{C}_{leq}(\mathbf{p}) \leq 0$

$\mathbf{C}_{eq}(\mathbf{p}) = 0$

where $\mathbf{p}$, a 4 by 6 matrix of 6 Laguerre coefficients of the control input for each of the 4 MPC-controlled joints, is the design variable and $\mathbf{C}_{leq}$ and $\mathbf{C}_{eq}$ are nonlinear inequality and equality constraints, respectively. Laguerre functions are a set of orthonormal basis functions, and are used to parameterize the control inputs which allows for smooth moment function profiles and prevents discontinuities [31]. The process of control input parameterization for Discrete MPC (DMPC) is described in greater detail in Appendix A, but the full derivation is outside of the scope of this thesis. What is necessary to note here, however, is that the optimization problem *at*

each time step (approximately twenty iterations in DS and 40 in SS), is 24-DOF (four MPC joints with six Laguerre function coefficients each) and nonlinear.

This thesis proposes many changes from the Sun Model [31], [32] optimization targets and model constraints as described in the following sections, primarily affecting the "Optimization" process of Figure 3.4, which consists of the design optimization problem discussed.

3.3.1 Sun Model Targets and Constraints

The Sun model optimizes joint angle trajectories to meet a desired step length during SS period of gait and target center of mass (COM) velocity at toe-off during the DS period [31], [32]. Additionally, the Sun model employs only endpoint MPC, meaning that the control algorithm compares only the final state to a target: terminal cost dominates the objective function [31]. The Sun model deviates from expectations of CNS behavior in two ways; the model optimizes only according to the final states of the system and only to meet a target step length for SS and COM velocity for DS.

In SS the Sun model optimization target is step length. The swing heel is constrained to contact the ground at the end of the prediction horizon, heel strike (HS), and cannot contact the ground before then. [31]. During DS period the optimization target is the sagittal forward velocity of the pelvis at toe-off (TO). The feet, subject to ground reaction forces (GRF), are unable to pass through the ground [31]. The end of each period is determined by the prescribed length of each finite prediction horizon.

3.3.2 End-Point Targets and Constraints

New constraints were implemented to the plant model simulation in this thesis to improve the prediction of the simulation framework between periods of gait. The end-point targets of the Sun model [31] are retained. This thesis proposes prediction and control horizons that extend beyond the length of the period but recede until a condition is met within the plant simulation. This method allows greater prediction capability than prior work by Sun [31] and van der Kooij et al. [33] as the time for the period is not pre-determined by the use of a final optimization state.

Double Support End-Point Targets and Constraints

DS employs a velocity end-point optimization target. The Sun model first proposed an end point-velocity target, but only in the forward sagittal direction [31]. This thesis uses a target velocity of the pelvis in both the forward and upward direction in the sagittal plane. The forward velocity matches the self-selected walking speed of the subject, and the upward velocity used was published by Winter [39]. The upward velocity of the pelvis at TO is generated by joint velocities that are crucial as initial conditions to SS period, as shown by Mena et al. [24] and Mochon and McMahon [26]. A DS prediction horizon was applied that exceeds 12% of the average gait cycle period [28] for each subject. The plant simulation and the period is constrained to end when there exists no GRF on the lag toe.

Single Support End-Point Targets and Constraints

SS retains a step length end-point optimization target, consistent with the Sun model [31], but adds a constraint that prevents the toe from passing through the ground. The SS prediction horizon also exceeds 38% of the average gait cycle period [28] for each subject. The period ends when heel strike of the swing foot occurs within the control window.

3.3.3   New Optimization Targets

The Sun Model does not accurately predict the transitions between periods of the GC and thus, can only predict one half of a GC. Therefore, gait analysis of the Sun Model requires the assumption that gait is symmetric [31], [32], limiting the usefulness of the prediction. This thesis uses much of the existing control framework developed by Sun but proposes new optimization criteria and model constraints to flexibly predict a complete GC without a symmetric gait assumption. As discussed in Section 2.4, the literature provides support for optimization criteria related to metabolic cost. Additionally, it is believed that CNS control is continuous, optimizing the majority of the cycle, rather than only end targets between periods. The following sections describe the application of new optimization targets and model constraints within the control framework.

COM Energy Optimization Criterion

Because the plant model is a kinematic and kinetic model rather than neuromuscular, a mechanical energy cost measure should be used rather than a calculation of metabolic cost [7].

This calculation can be done in one of two ways: minimizing the work done on the body's center of mass or minimizing the work done on the body segments. Burdett et al. demonstrated that though the work done on the COM is a less accurate predictor of mechanical work, it is more highly correlated with metabolic cost [7]. Thus, minimization of COM energy is the optimization target that aims to reduce metabolic cost and can be calculated as

$$E_{COM} = mgh_{COM} + \frac{1}{2}mV_{COM}^2 \ , \tag{3.1}$$

and

$$\dot{W} = \sum \Delta E_{COM} \ , \tag{3.2}$$

where E_{COM} is the potential and kinetic energy of the body's COM, m is body mass, h_{COM} and V_{COM} refer to the height and velocity of the body's COM, and $\dot{W}$ is the work done to the COM, calculated at each time step of the prediction horizon.

Dynamic Effort Optimization Criterion

Dynamic effort is defined as the sum of all joint torques over time, classified as an "effort-like" optimization criterion [3], and can be calculated using

$$M = \sum \tau_i^2 \ , \tag{3.3}$$

where M is the dynamic effort and τ_i is the torque at each joint, excluding passive elements. Note, the calculation of these moments is independent of the ordinary differential equation solver's adaptive step size, ensuring that the same number of points are used in each optimization.

3.3.4 Weighted Sum Multi-Objective Optimization

Incorporation of multiple optimization criterion into the same cost function requires MOO methods for the model to achieve multiple end-point targets simultaneously. These control objectives can also be weighted within the objective function to achieve normal gait. A variety of MOO methods were considered as published by Marler and Arora [21] and a weighted sum approach was chosen for its simplicity with the gradient-based solution method used in the Sun Model [31], [32]. Since the goal is to minimize the objective function, each optimization target can simply be summed together with appropriate weighting coefficients, determined experimentally

Table 3.2: Description of subject data used.

	Subject 1	Subject 2	Subject 4
Collected by	Author	Author	Sun [31], [32]
Collected at	OREC Gait Lab [2]	OREC Gait Lab [2]	MCW CMA [1]
Motion Capture System	Qualisys	Qualisys	Vicon
Data Processing	Visual3D	Visual3D	Unknown
Kinematic Data	Yes	Yes	Yes
Kinetic Data	Invalid*	Yes	Unknown

*Force plate data was not collected.

in future work. This concept was demonstrated successfully by Karimian et al. within an MPIC simulation framework [17].

3.4   Model Anthropometry and Simulation Evaluation

Kinematic and kinetic gait data of three normal ambulators (Table 3.2) are used to evaluate model performance in this thesis. Subject anthropometric data is also used to parameterize the models within the simulation framework. For *new* subject models generated in this thesis (Subjects 1 and 2), all model sizing parameters were directly measured and segment masses, moments of inertia, and location of COMs were calculated using Winter's equations and data [39]. For Subject 4 [31], segment lengths were directly measured, but other sizing parameters which do not affect the equations of motion were estimated, while segment masses, moments of inertia, and COM locations were calculated with Winter's data [39].

Subject 4 refers to the Sun Model, used as a baseline in this thesis, which is parameterized according an 86.8-kilogram body mass and 1.90-meter height [31]. Model anthropometry was inherited in the Sun plant and internal models. Limited motion capture data from Subject 4 analysis is available. Motion capture data was collected in the Medical College of Wisconsin (MCW) Center for Motion Analysis (CMA) with a Vicon motion capture system. Data processing methods are unknown, and only kinematic data is available for this thesis.

Subjects 1 (85.7-kilogram mass, 1.83-meter height) and 2 (78.0-kilogram mass, 1.78-meter height) refer to subject gait studies conducted by the author in the OREC Gait Lab [2]. 3D Motion Capture Gait Analysis protocols were conducted for this thesis with IRB approval. Data acquired during these sessions includes: bilateral anthropomorphic measurements, lower limb kinematics, and kinetic data.

Table 3.3: Description of anthropometric measurements.

Measurement	Landmark Description of Measurement
Inter ASIS Distance	distance from left and right anterior superior iliac spine (ASIS)
Leg Length	distance from ASIS to lateral malleoli
Thigh Length	distance from greater trochanter to lateral femoral epicondyle
Knee Diameter	distance from medial to lateral femoral epicondyle
Ankle Diameter	distance from medial to lateral malleoli
Thigh Proximal Circumference	circumference just distal to ischial tuberosity
Thigh Distal Circumference	circumference just proximal to the patella
Foot Length*	distance from calcaneal tuberosity to distal end of hallux
Foot Width*	distance from first metatarsal head to fifth metatarsal head
Foot Rocker*	distance from calcaneal tuberosity to first metatarsal head

*Measurement made on AFO instead of subject

The motion capture and data processing protocol for Subjects 1 and 2 is presented in detail in the following sections. Motion capture data was recorded of subjects walking both unhindered (normal case) and with a rigid AFO (pathological) to inhibit ankle flexion. Data for Subject 4 was collected and processed by Sun, and is presented in his dissertation [31]. The data collected is used in evaluation of the simulations developed in this thesis.

3.4.1 Anthropomorphic Measurements

For each GC simulation, the plant and internal models are parameterized according to subject anthropometry, using both subject measurements and approximations as a percentage of subject height or bodymass from Winter's published data [39]. The anthropometric measurements taken of each subject during the gait testing session, height, weight, orthosis mass, bilateral length and circumference, are summarized in Table 3.3.

Model parameters adjusted for each subject include limb lengths, radii, masses, and inertias, and are listed in Appendix B with their conversion from subject measurements. Anthropomorphic data for each subject is presented in Appendix B.

3.4.2 Motion Capture Protocol

Fifteen reflective markers were placed bilaterally according to a Modified Helen Hayes marker model (Figure 3.6) on Subjects 1 and 2. The lateral malleolus and heel (calcaneal tuberosity) markers were placed over the AFO on the right leg for pathologic gait trials. Motion capture was collected for overground walking trials for the normal and AFO (pathologic) case. All trials were collected at self-selected walking speed.
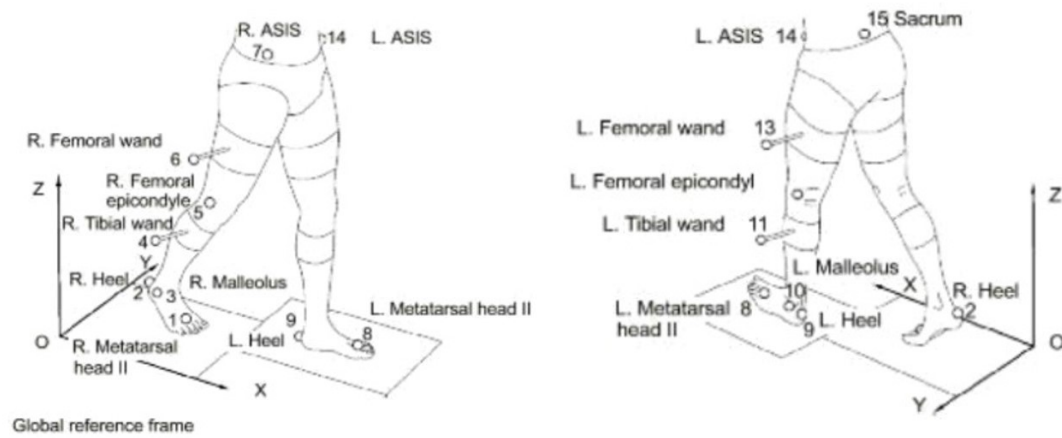
Figure 3.6: Modified Helen Hayes marker model used for 3D Motion Capture [2].

Kinematic data was collected at 120 Hz using a 10-camera Qualisys motion capture system, and kinetic data were captured at 1200 Hz with an AMTI force plate embedded in the level walkway.

The Qualisys motion capture system was calibrated and a static trial was collected with the subject standing centered on the force plate. Knee-alignment devices (KADs) were used at the knee in place of the knee marker during static trials (Figure 3.7). The KADs were replaced with knee markers and the subject walked at self-selected speed over the walkway and force plate. Trials were repeated until six clean heel-strikes, shown in Figure 3.7, had been measured at the force plate, three with each leg. The subjects then donned a rigid AFO fit for their right leg, markers were reattached to the outside of the AFO at the lateral malleoli and calcaneal tuberosities, and the subject was given up to ten minutes to acclimate to the new condition. Static trials with KADs and six dynamic trials with clean HS were captured with the AFO condition.

3.4.3   Motion Capture Data Processing

Kinematic and kinetic data processing of 3D motion capture data requires conversion of marker data from 2D to 3D, application of subject-specific kinematic models, HS and TO event detection, computation of joint forces and moments from ground reaction data (force plate), and averaging of gait cycles. Because the simulation proposed in this thesis is constrained to the sagittal plane, kinematic and kinetic joint motion and moments used in evaluation of the model are limited to sagittal plane data.

Static Trial Markers with KAD   Dynamic Trial Markers
Subject demonstrating "clean" HS
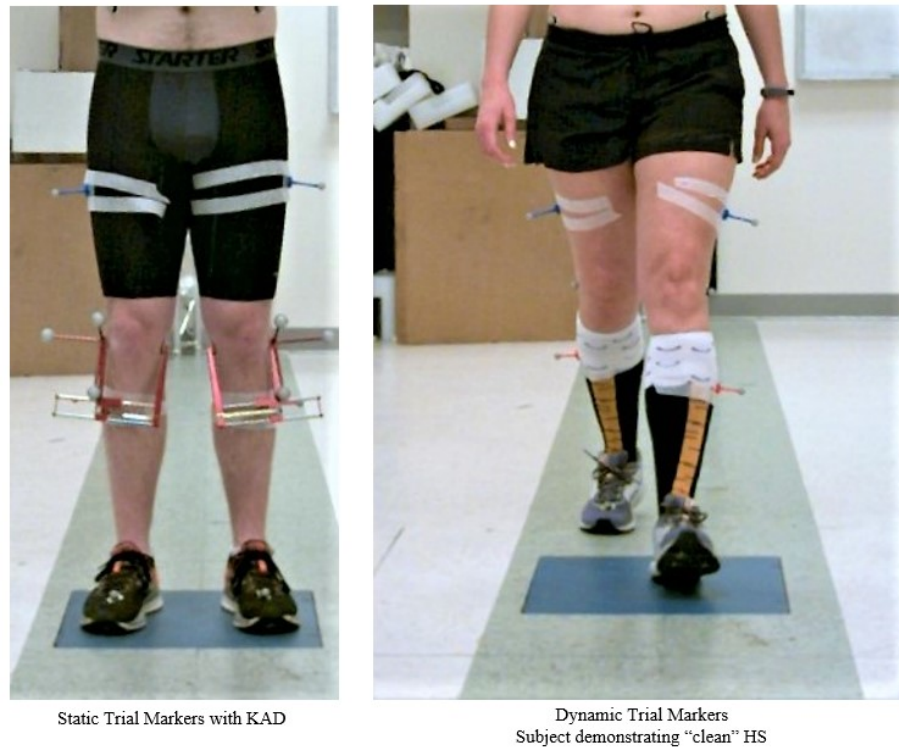
Figure 3.7: Placement of markers during static and dynamic trials.

Using a custom data processing pipeline for the Qualisys Motion Capture system from the OREC Gait Lab [2], 2D marker motion data from each camera was converted to 3D, GC events were automatically detected and joint forces and moments calculated using force plate data, and a full gait report (kinematics and kinetics plots) was generated for Subjects 1 and 2. The gait report output is a standard clinicial format (data presented for sagittal, coronal, and transverse planes) with all measured GCs reported from 0 to 100% of the GC. Full gait reports for Subjects 1 and 2 are presented in Appendix B. A full gait report is unavailable for Subject 4, but sagittal joint angle trajectories are presented in B and are used in evaluation of Subject 4 specific simulations.

For this thesis, subject-specific GC or period simulations are compared to the measured sagittal plane data. Thus, sagittal plane trajectories were imported to MATLAB, averaged, and plotted against simulation results.

3.5 Simulation Evaluation

Data collected according to the procedures described above is used as a baseline from which to evaluate simulation performance. This evaluation is made in this thesis consistent with

observational methods used in clinical gait analysis.

Though it is possible to use an root-mean-square error measure of the difference between simulated and measured trajectories, observational analysis remains the best method of evaluation for gait data because it allows the clinician to identify gait abnormalities that present as magnitude shifts, temporal shifts, and/or change in dynamic range. With this "impairment-focused interpretation" [6] of gait analysis, the assumed intent is to identify factors that limit walking ability, rather than just quantifying the amount of difference. In the case of this thesis, observational clinical analysis seeks factors that limit the capacity of the model and simulation framework to predict normal walking patterns.

If only an RMSE value is used, information is lost about specific "impairments" and their relation to other features of the gait pattern. This interconnectedness of gait features is common because of the relative angle standards of data presentation. Additionally, an RMSE value may actually provide information contrary to what would be derived from observational analysis, with magnitude or temporal shifts. For this reason, simulation data generated in this thesis was evaluated clinically with measured gait data as a reference.

3.6   Summary

The gait simulation framework used in this thesis is an expansion of the Sun model [31], [32]: a seven-link, nine-DOF, forward dynamic human gait model with a control system that is primarily Model Predictive Control (MPC) with secondary classical feedback control (PID). This control method allows for constraints such as joint torque limits, range of motion limits, etc., to direct the simulation of gait without any prior knowledge of gait or joint trajectories. The gait simulation framework includes two plant models, two internal models, an objective function for each period (SS and DS) of gait, and a common optimization framework for both phases.

MPC uses the simplified internal models to control joint angle trajectories of the plant by optimizing joint moments to a cost function which includes both optimization *targets* and *constraints* to predict walking patterns. Optimization targets are components of the cost function which the framework aims to minimize in its prediction of control inputs. The optimization constraints may be *physical* constraints such as joint limits, or *characteristic* constraints, which could dictate the end state of a simulation period.

New constraints were implemented to the plant model simulation in this thesis to improve the prediction of the simulation framework between periods of gait. This thesis uses a target velocity of the pelvis in both the forward and upward direction in the sagittal plane in DS, and constrains the toe to not pass through the ground in SS, in addition to the HS characteristic constraint in SS employed by Sun [31], [32]. New optimization targets, work on the COM and dynamic effort, were applied.

Kinematic and kinetic gait data of three normal ambulators are used to evaluate model performance in this thesis, and subject anthropometric data is also used to parameterize the models within the simulation framework. Anthropometric measurements were taken and motion capture data was recorded of Subjects 1 and 2 walking both unhindered (normal case) and with a rigid AFO (pathological) to inhibit ankle flexion. Motion capture data and anthropometric measurements of Subject 4 are adopted from Sun [31], [32].

CHAPTER 4

RESULTS

With the simulation framework proposed, prediction of a subject-specific GC consists of four consecutive period simulations, DS, SS, DS, and SS. To simulate a GC the initial conditions (IC) for the first DS simulation are taken from the Sun Model [31] or subject data, but each of the periods should use the end states of the prior period as an IC set. This pattern mandates that the transition between simulation periods are marked by TO and HS events if the simulations obey period constraints, as they are in a normal gait cycle. Additionally, simulation of a full GC requires that the final states of one period are suitable IC for the next.

4.1   Baseline GC Simulation

To create a baseline GC simulation (DS, SS, DS, and SS) representative of the Sun cost functions [31], [32], subject-specific models were created for Sun Subject 4, and the Sun optimization targets (step length and COM velocity at TO) were used in the cost function [31]. New constraints (those proposed in Section 3.3.3) were applied to the simulation framework which specified that the final states of one period must be the initial states of the following period. Additionally, each period was constrained to end upon HS or TO for SS or DS, respectively, if the event occurred prior to the prescribed length of the prediction horizon. This additional constraint increases the predictive capability of the Sun framework [31], [32] since it allows GC events to dictate the length of the period.

Joint angle trajectories of this baseline continuous simulation compared to Sun model results [31] and Subject 4 measured joint trajectories are shown in Figure 4.1. Consistent with gait analysis conventions, the trajectories are shown from HS to HS of one limb from 0 to 100% GC. Vertical lines denote TO for each trajectory. For the simulated data, the start of the second SS phase is marked with a vertical line where TO should occur.

Initially, the Sun model appears to be a better approximation of the subject data than the baseline simulation proposed. However, large jump discontinuities occur at the transitions between DS and SS because the full GC was assembled from pieces of the simulated half GC. These discontinuities illustrate the need for continuous transitions from period to period and that simulation of a half GC is insufficient for the evaluation of optimization targets and controller performance. Though achieving continuity over four periods is an improvement upon the Sun
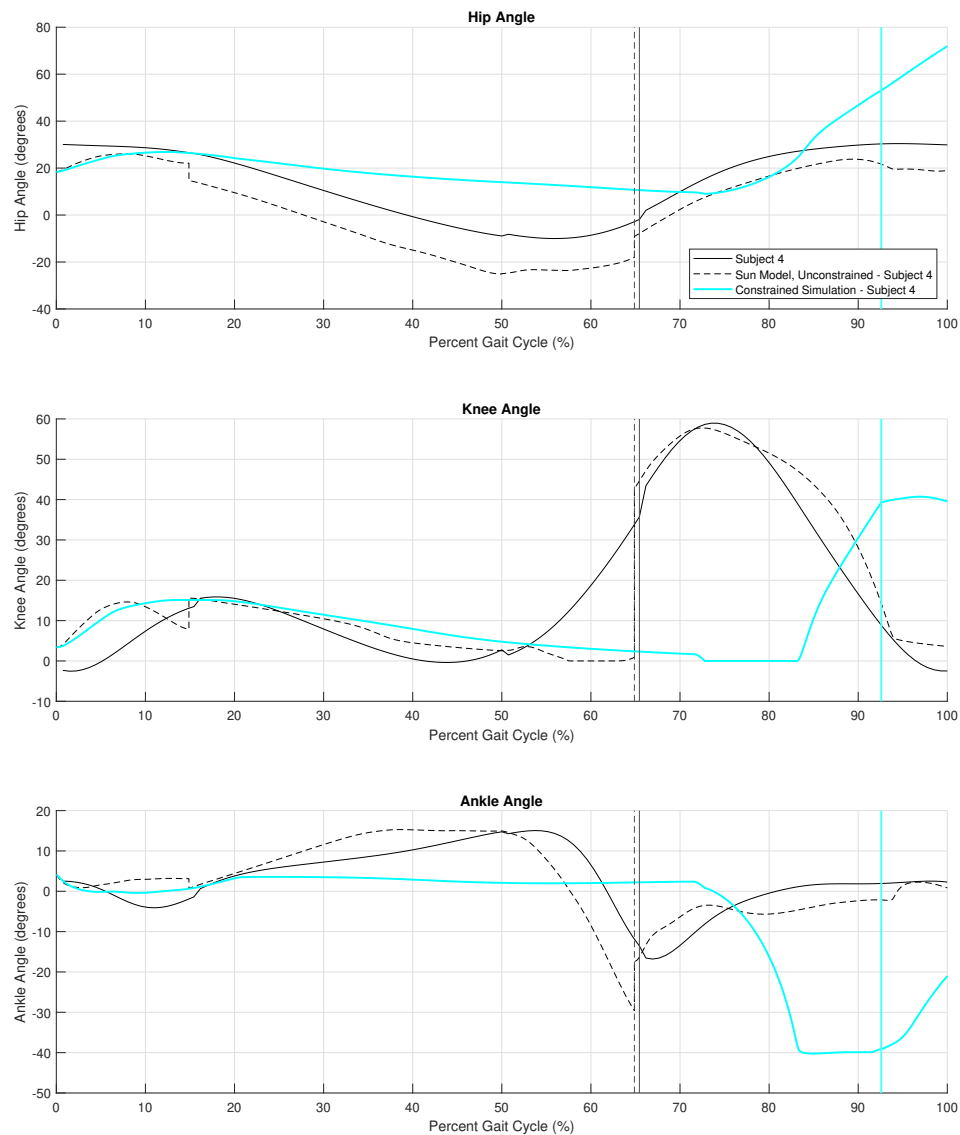
Figure 4.1: Subject 4 simulated and measured sagittal plane joint angle trajectories over the GC.

model, which originally only simulated a half GC over SS to DS [31], the simulated trajectory diverges from the Subject data early in the stance phase, where the first transition from DS to SS occurs.

The resulting gait pattern from the baseline GC simulation, which illustrates the kinematics of the model resulting from joint angle trajectories in Figure 4.1 over the first DS and SS periods, is shown in Figure 4.2. This pattern clearly illustrates the failure of the simulation to achieve HS of the swing leg during mid-stance because no HS occurs. Thus, by the second DS phase, the simulation is too divergent from subject data for the controller and optimization to recover. Because of the missed HS and the necessary continuity of the GC, the rest of the simulated trajectory does not have any physical significance.
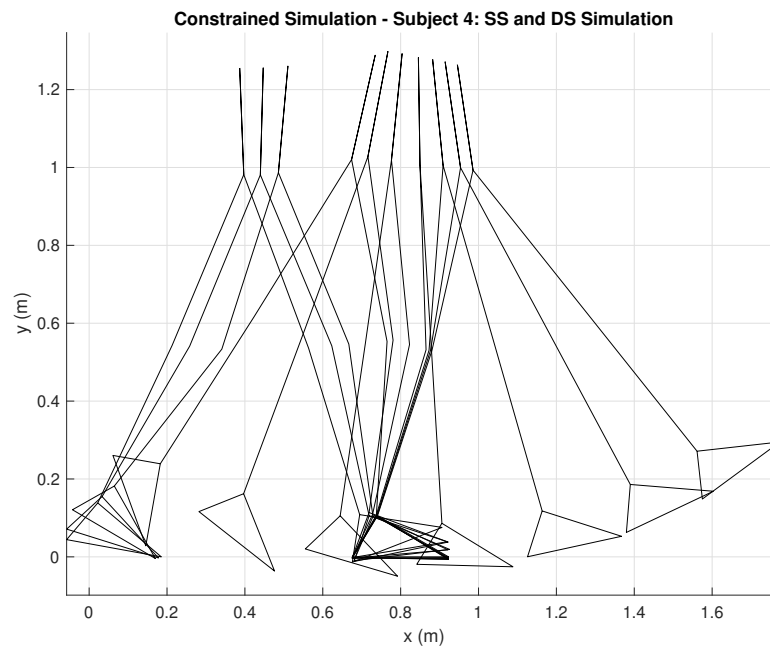
Figure 4.2: Subject 4 simulated walking pattern over DS and SS period.

Therefore, applying the new constraints (Section 3.3.3) to the Sun model did not result in a full GC marked by TO and HS. This limitation is seen primarily in the transition from DS to SS, as no simulations successfully completed the target step length in the first two periods because the heel did not contact the ground. Thus, the simulated GC was not marked by TO and HS, but the new constraints did allow the simulation framework to generate a C_0 continuous simulation of all four periods consecutively, which was not achieved with the Sun model [31], [32]. Without successful, repeatable simulation of SS period, a full GC simulation is infeasible.

Table 4.1: Kinematic Conditions for IC Study.

Trial	Step Length	Pelvis x (m)	Pelvis y (m)	Pelvis Forward Velocity (m/s)
1	0.7345	-0.13616	1.0699	1.3854
2	0.7345	-0.42001	0.94032	1.3854
3	0.7345	-0.41074	0.97891	1.3854
4	0.7345	-0.37112	0.95663	1.3854
5	0.7345	-0.34705	0.94385	1.3854
6	0.7345	-0.28047	0.95938	1.3854
7	0.7345	-0.31293	0.98134	1.3854
8	0.7345	-0.34632	1.0152	1.3854
9	0.7345	-0.27879	1.0461	1.3854
10	0.7345	-0.25003	1.0223	1.3854
11	0.7345	-0.22071	1.0062	1.3854
12	0.7345	-0.16941	1.0352	1.3854
13	0.7345	-0.18462	1.0808	1.3854
14	0.7345	-0.17836	1.0612	1.3854
15	0.7345	-0.16389	1.0417	1.3854
16	0.7345	-0.15901	1.0819	1.3854
17	0.7345	-0.18873	1.0486	1.3854
18	0.7345	-0.36360	0.97193	1.3854
19	0.7345	-0.23249	1.0283	1.3854
20	0.7345	-0.4541	0.95468	1.3854

Three potential barriers to a successful simulation of the first SS period were identified: initial conditions, unexpected joint actuation behavior, or insufficient solution-finding methods. Because it is difficult to separate the effect of the optimization from the rest of the simulation framework, experiments were run to examine the barriers to the framework which can be isolated. The following two sections describe these experiments conducted to better understand the limitations of the SS period simulation, which examine the sensitivity of the model to initial conditions and joint actuation.

4.1.1 SS Initial Condition Study

As illustrated in the prior section, to achieve a full GC, SS period must start from TO, or the final states of DS, and advance the simulation through HS. Simulating this period transition, however, requires the IC of SS drastically different than the Sun model, which began SS with the swing foot raised above the ground to utilize gravity to advance the swing leg [31]. Because literature has shown that simulated SS periods are highly dependent on initial conditions [26], [19], in order to identify a region of IC which allows for successful completion of SS period a series of SS simulations were run with IC sets which met the pelvic position (relative to stance heel) and forward sagittal velocity kinematic conditions listed in Table 4.1.
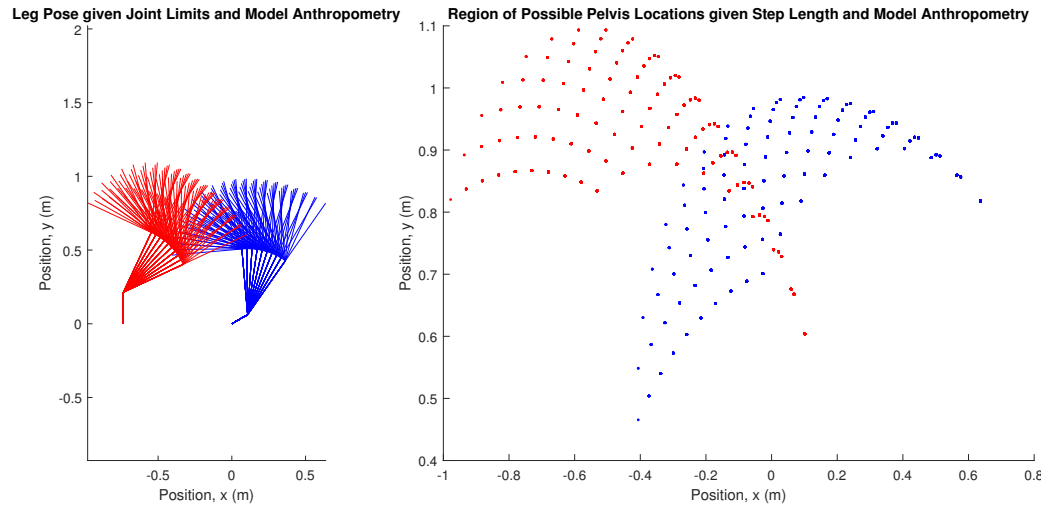
Figure 4.3: Region of possible pelvic axis positions given subject anthropometry and prescribed step length.

The IC sets (the sets of joint positions and velocities for each simulation) were derived from an inverse kinematic analysis to identify the region of possible pelvic positions for a subject given a specific step length and pelvic velocity (Figure 4.3). This was achieved by using fixed foot positions and sweeping through the range of motion (ROM) at the ankle and knee joints for each leg. With this method each leg has a region of possible locations for the pelvis, since the pelvis of the gait model is an axis, rather than a rigid body. The region of possible pelvic positions, where the red (swing leg hip) and blue (stance leg hip) markers overlap was discretized, and for a specified step length at TO it is relatively small. The IC sets chosen for this study were generated by inverse kinematics from 20 pelvic axis positions which spanned the allowable space.

Simulations with all IC cases resulted in either a premature HS or a tripping motion: no simulations achieved the target step length. Figure 4.4 shows one simulation which exhibits premature HS, meaning that HS occurred in mid-swing before the swing leg advanced past the stance leg. Additionally, some solutions resulted in unstable gait, resembling a tripping motion shown in Figure 4.5, where the stance leg was unable to support the forward motion of the HAT. Resulting simulations did not end in a suitable pose for DS to begin because none met the target step length.

No simulation met the optimization targets or model constraints, despite testing 20 IC sets which spanned the discretized space. Assuming some continuity within the region of

SS Simulation - Subject 04: SS and DS Simulation
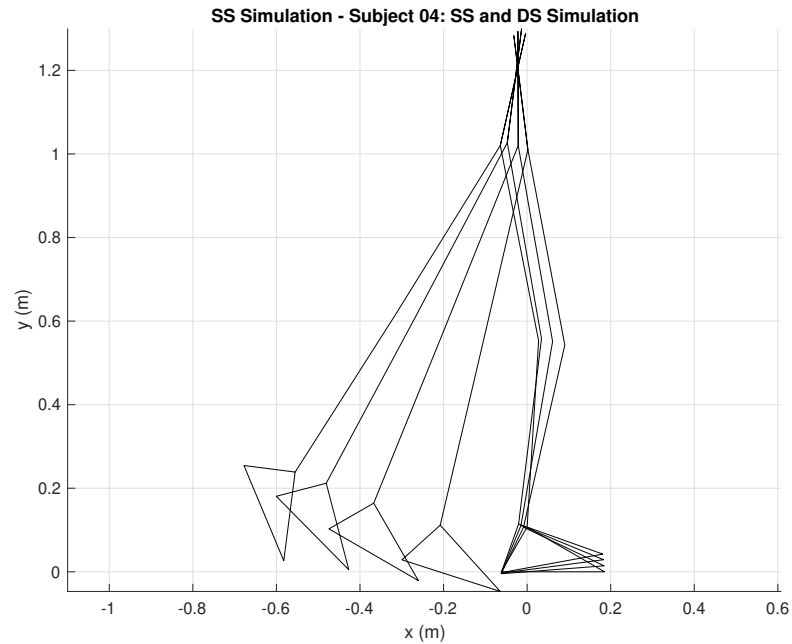
Figure 4.4: Subject 4 simulated gait over SS period resulting in premature HS.

allowable pelvic positions, it is likely that no IC set from the space would have resulted in successful simulation. Regardless of the IC set applied, the simulation framework finds basically one of two solution types, shown in Figures 4.4 and 4.5. Because no simulation was successful, or even varied from other solutions as a result of a different IC set, the failure to successfully simulate SS in this experiment is not likely due to an inappropriate choice of IC. As discussed in Section 2.2, literature has shown that SS is heavily dependent on the set of IC applied [19], [26]. Because this IC set dependence was not observed in the simulation, and a successful SS period simulation could not be achieved with *any* IC set, it is likely that a different component of the simulation framework is the barrier. However, it should be noted that, although IC set choice may not be the cause of failure in this thesis, IC set choice will likely have significant effect on the solution when the optimization framework is corrected.

4.1.2 SS Torque Actuation Study

The SS IC study described in Section 4.1.1 demonstrated that the failure of the model to meet period constraints in SS is most likely not dependent on IC. In fact, solutions with varying IC sets often resulted in highly similar solutions, pointing instead to unexpected joint actuation
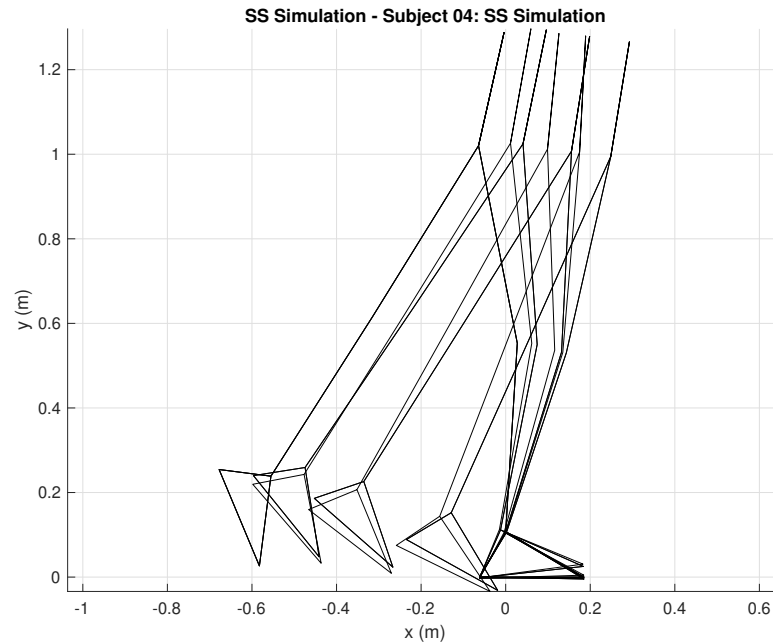
Figure 4.5: Subject 4 simulated gait over SS period resulting in tripping.

behavior or insufficient solution-finding methods.

To better understand the failure of the model to meet constraints in SS and the effect of joint actuation on the model, several simulations were run to illustrate model sensitivity to each of the five joint torque sources. As detailed in Section 3.1, several passive and active torque sources are used within each joint, but only the Laguerre function formulation is directly controlled by the MPC scheme. A set of SS simulations were run which separate the effects of the torques by removing different layers of torque sources. This set of simulations consist of the majority of torque combinations that would likely interact when acting upon the joints.

Sagittal plane joint angle trajectories for SS period with the following joint actuation cases are shown in Figure 4.6:

1. no joint actuation (Joint Actuation Off),

2. passive internal spring and damping torque only (Passive Actuation Only),

3. passive spring and damping torque, joint limit torques, and hard stop torque only (MPC Actuation Off),

4. passive, joint limit, and hard stop torques with subject specific base torque polynomials (Laguerre Off),

5. passive, joint limit, and hard stop torques with Laguerre function control action (Base Polynomials Off),

6. joint limit and hard stop torques with base torque polynomials and Laguerre function control action (Passive Actuation Off),

7. and passive and hard stop torques with base torque polynomials and Laguerre function control action (Joint Limit Actuation Off).

Each simulation was run for SS period with a step length target as both a model constraint and optimization target to eliminate the possibility of conflicting goals within the optimization routine. This combination ensured that the only goal of the simulation was to achieve HS at the specified step length. Each simulation was run from an IC set consisting of the final states from a Subject 2 DS simulation as would happen in simulation of a full GC, which began from Subject 2 gait data. The gait model used was parameterized by Subject 2's anthropometry (Appendix B), which allowed for a polynomial fit of subject-specific torque data to be used as the initial guess within the MPC control action formulation using subject-specific torque data, rather than generalized data from Winter [39] which is required for Subjects 1 and 4 in the absence of subject-specific torque data. Because this torque data is taken directly from analysis of subject gait, it is the best available starting point for the optimization routine.

For SS period, stance ankle, swing ankle, swing knee, and swing hip are MPC controlled, so changes in joint actuation are only applied within these four joints. Two joints are of particular importance during SS period: stance ankle, which provides the base of the inverted pendulum motion as the COM shifts over the stance leg, and swing hip, which drives the swing leg forward and provides braking when approaching HS.

Figure 4.6 demonstrates that the two most dominant components of model joint torques are the passive spring and damper moments and the base torque polynomials because the simulations actuated by only these components comprise the two solution types. This dependence is observed in that simulations which include one or both of these torques yield solutions nearly identical to simulations that *only* include those torques, i.e., MPC Actuation Off is the same as the simulation with Base Polynomials Off.

Joint limit actuation, however, (both nonlinear regions of joint spring and damping and the mechanical "hard stop" within the joint) functions as expected, preventing the model from exceeding the joint limits. This behavior is observed in Figure 4.6 by comparison of the un-actuated case with simulations employing passive actuation where the slope of position curves

Subject 2 Gait Simulation Joint Angle Trajectories over Single Support Period
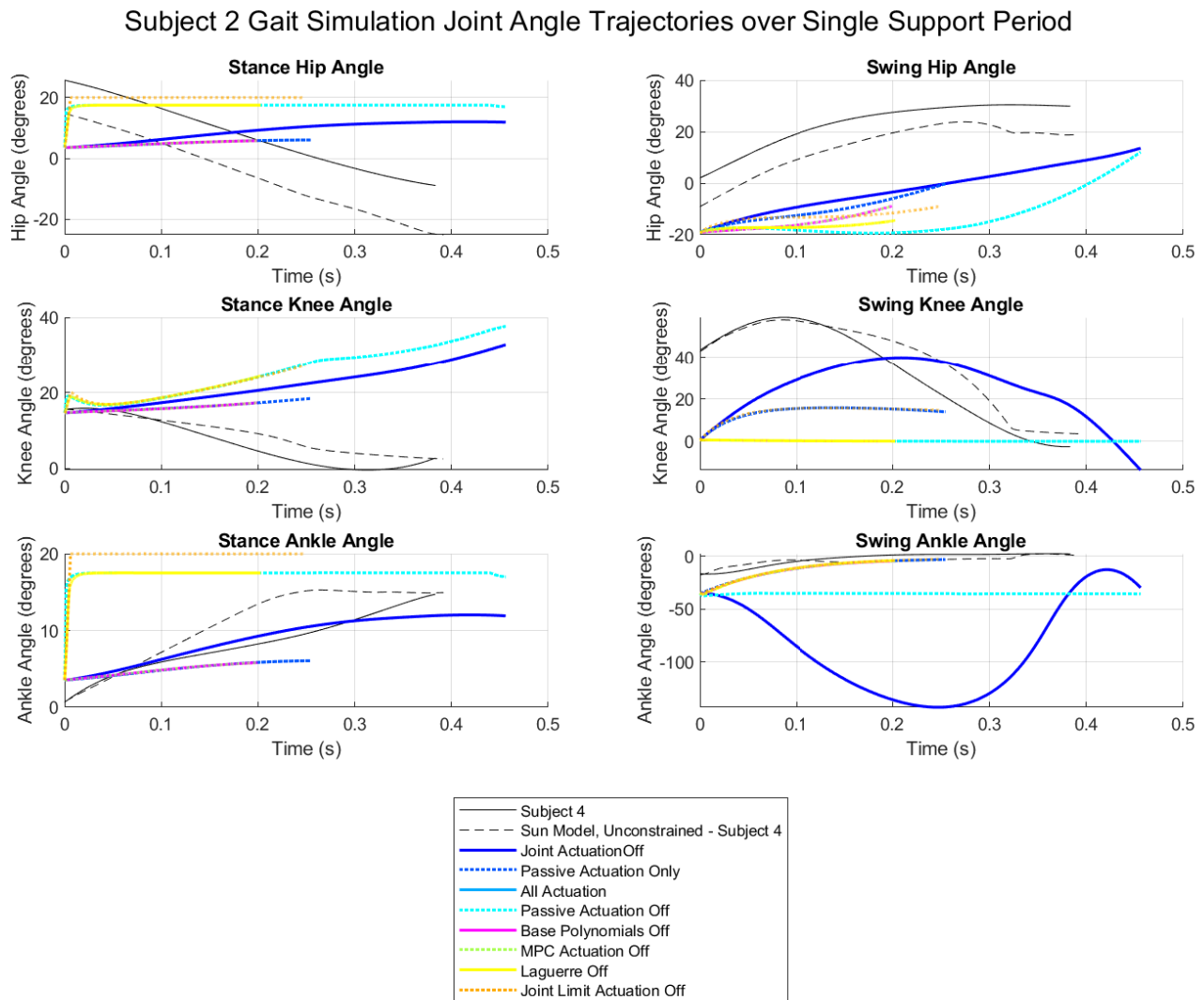
Figure 4.6: Subject 2 simulated sagittal plane joint angle trajectories for SS period with varying joint actuation cases.

change drastically around normal joint ranges of motion, particularly in the stance hip and ankle. In most simulation cases these moments do not affect the solution.

Of greatest concern however, is the simulation framework's insensitivity to "active" joint actuation, or the actuation dictated by the controller. Whether the Laguerre function formulation, which makes up the control action, is included or not, the resulting joint angle trajectories are the same (All Actuation and Laguerre Off trajectories lie on top of each other). Though this insensitivity could be caused by the Laguerre coefficient initial guess, increasing the coefficient initial guess by two orders of magnitude yields nearly identical solutions (Figure 4.7). Thus, it can

be concluded that the MPC control action currently has negligible effect on the SS period simulation because the optimization cannot find a solution which meets the model constraints.

In addition, the simulation framework finds alarmingly similar solutions within this study for such varied actuation cases. The solution space for the SS optimization is 24-dimensional *at each time step* of the prediction horizon. With such a high-DOF solution-space, the primary problem with the findings of this set of simulations is that the simulation, when the model is actuated, finds one of two solutions (neither of which meet model constraints during SS). The optimization results also do not change throughout iterations of MPC control. With the only constraint being that the heel should clear the ground during until HS, it is highly improbable that the optimization is over-constrained. It is therefore more likely that the optimization algorithm is not an appropriate choice for the class of optimization problem presented in SS.

The optimization routine used, fmincon, uses MATLAB's Interior Point algorithm [23]. The algorithm is a nonlinear gradient solution method, but finding a solution to the optimization problem is more difficult with inequality constraints (the constraints used in Sun's work [31] and this thesis) than equality constraints and is not appropriate for non-convex optimization problems. Without a way means to visualize such a large-DOF solution space, it is difficult to ensure convexity and smoothness. Further experimentation will be necessary to properly classify the optimization problem. If the optimization problem can be classified, an appropriate solution algorithm could be chosen which could reliably find a solution for any given set of constraints and IC, which would then allow the simulation framework to reliably meet model constraints for SS. Classifying the optimization problem and identifying an appropriate solution algorithm is outside the scope of this thesis, but could reinstate the MPC framework proposed by Sun [31] as a viable method of gait prediction and simulation.

4.2   Optimization Targets in DS

In contrast to challenges demonstrated in the simulation of SS that prohibit the simulation of a full GC, the proposed MPC framework does seemingly affect the solution more significantly in DS. Regardless the underlying cause of optimization success, simulations of DS allowed application of cost functions which employ the new optimization targets proposed in this thesis (Section 3.3.3).

DS simulations for models parameterized to Subject 4 [31] are shown in Figure 4.8, with the Sun optimization target (COM velocity at TO), change in COM Energy (work done to the
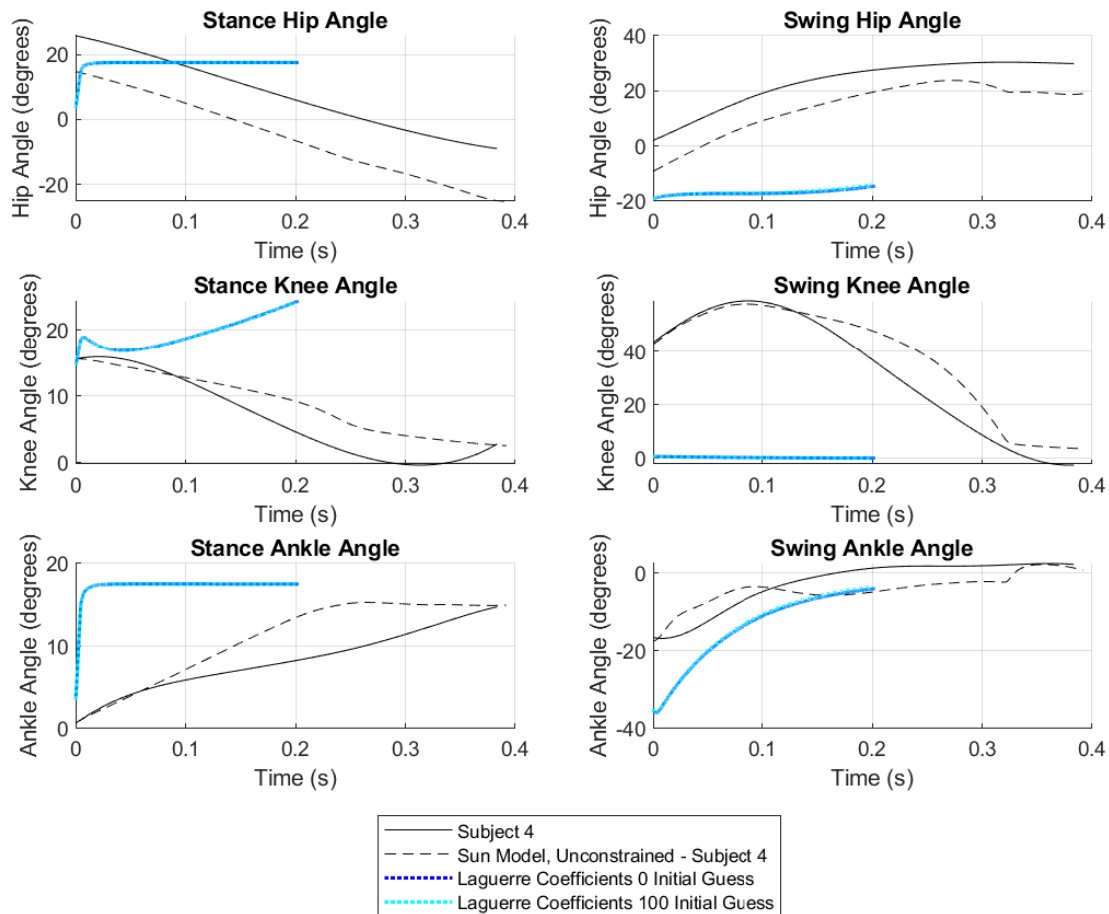
Figure 4.7: Subject 2 simulated sagittal plane joint angle trajectories for SS period with varying Laguerre Coefficient initial guesses.

COM), or dynamic effort in the cost function. Each optimization target within the cost functions is described in greater detail in Section 3.3.3. Note that ICs used in these simulations were chosen consistent with the Sun model's simulation of Subject 4 gait, so that a direct comparison can be made. As shown in Figure 4.8, variation of optimization targets within the cost function does have significant effect on the solution for DS. Not only does this variation of solutions confirm that the Laguerre function MPC control trajectory is not insignificant during the DS simulation, but demonstrates that the MPC framework can be successful when models are constrained to end upon GC marker. Two constraint cases are shown for each cost function, each a method to identify the TO event:

1. DS ends upon TO when GRF on the lag toe are less than or equal to zero, i.e., the ground reaction forces are holding the lag foot to the ground,

2. or DS ends upon TO when GRF on the lag toe are less than or equal to zero *and* the lead toe has made contact with the floor, i.e., the lead foot is flat.

The difference in simulation period length between constraint cases given a particular cost function points to the importance of appropriate characteristic constraint selection (defined in Section A.1). Because the simulations with constraints on both the lag toe and lead foot generated a period length more consistent with that of the normal ambulator data, the latter constraint condition was used for the rest of the DS simulations.

Of the simulations presented in Figure 4.8, the new cost functions proposed better approximate subject normal data for most joints. Of particular importance in DS is the lag ankle angle trajectory, where plantarflexion of the foot drives the lag leg to TO and into swing in the following period. The simulated trajectories from both dynamic effort and COM energy cost functions both approximate the stance ankle angle trajectory better than the Sun cost function. The simulations do diverge from normal ambulator data in both lag and lead hip angles, though in DS both hip angles are controlled by PID, and should not be considered in evaluation of MPC performance. Additionally, at TO lag knee flexion is better approximated by both COM energy and dynamic effort cost functions. Knee flexion and velocity at TO have been identified as IC that have significant influence on SS [19], [26]. Because SS is highly IC dependent, the best cost function for DS may be the one which achieves the most appropriate IC set for the following SS period, and thus should be considered in the evaluation of proposed optimization targets.

DS was also simulated for Subjects 1 and 2 with characteristic constraints applied to the lead and lag toe, i.e., TO occurs when the lead toe has made contact with the ground and when the lag toe leaves the ground, consistent with normal walking patterns observed [6]. As demonstrated in Figure 4.8, this constraint case also often leads to a longer simulation, which is closer to the period time measured in subject gait studies. An additional challenge was encountered in generating DS simulations for Subjects 1 and 2 because subject-specific joint angles (measured in subject gait analysis) at the beginning of the period did not meet kinematic requirements. For both subject models, subject-specific joint angles resulted in a model pose in which the lead foot was below the ground. Thus, DS IC sets for Subjects 1 and 2 were developed with modification from the Sun model DS IC for Subject 4. The IC sets were found by iterative adjustment of the lag ankle, because the lag foot is constrained to the ground as a planar joint in

Subject 4 Simulation Joint Angle Trajectories over Double Support Period
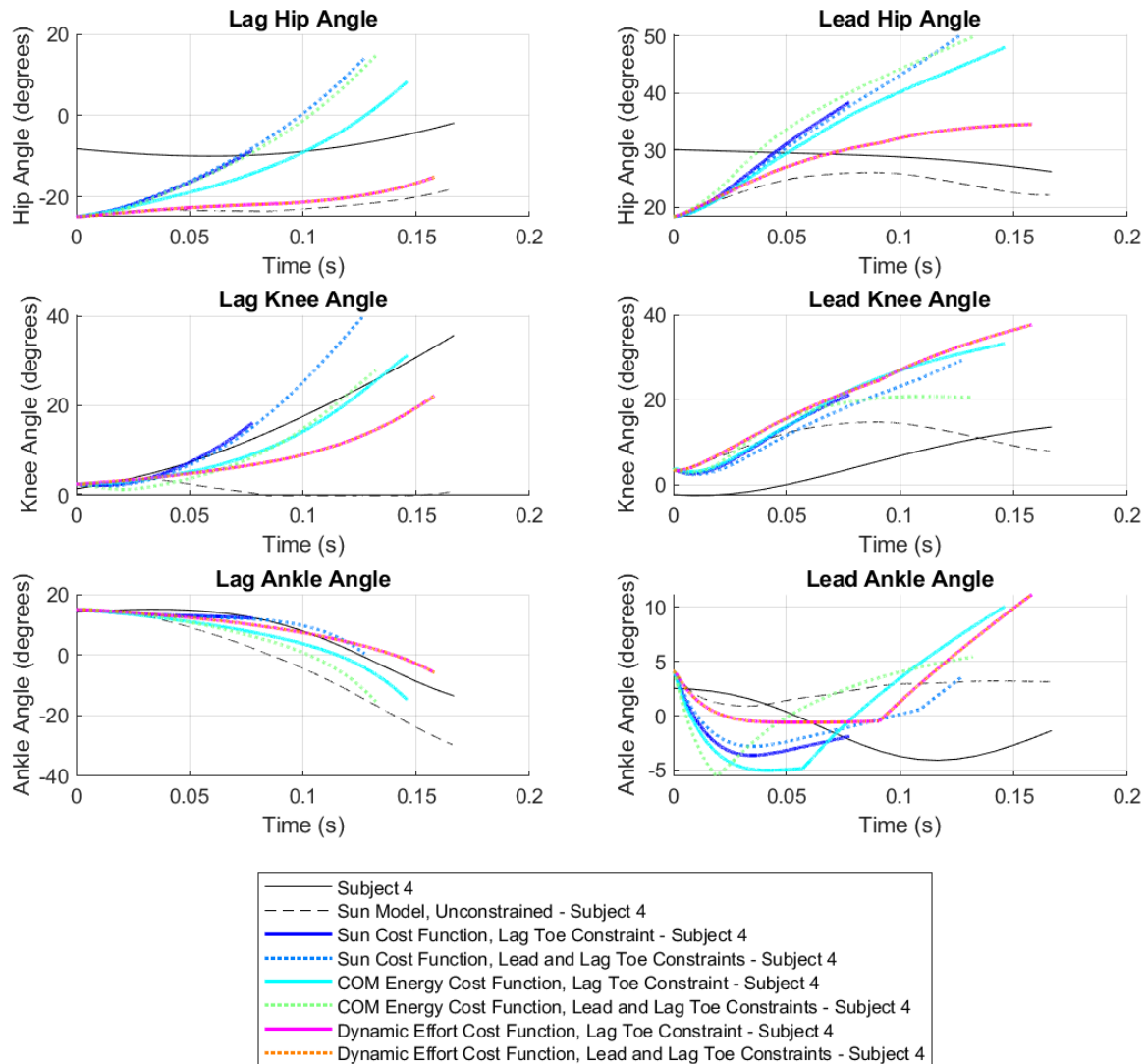
Figure 4.8: Subject 4 simulated sagittal plane joint angle trajectories for DS period with varying optimization targets.

the model framework. This adjustment and simulation was completed approximately 15 times for each model to identify a pose in which the GRF on the lead foot allowed successful optimization.

After identifying an appropriate IC set for each subject, DS was simulated for each subject with Sun, COM energy, and dynamic effort optimization targets. Resulting joint angle trajectories and subject measured gait data are shown in Figures 4.9 (Subject 1) and 4.10 (Subject 2). For most joints, simulated data diverges from measured subject joint trajectories in simulations for both
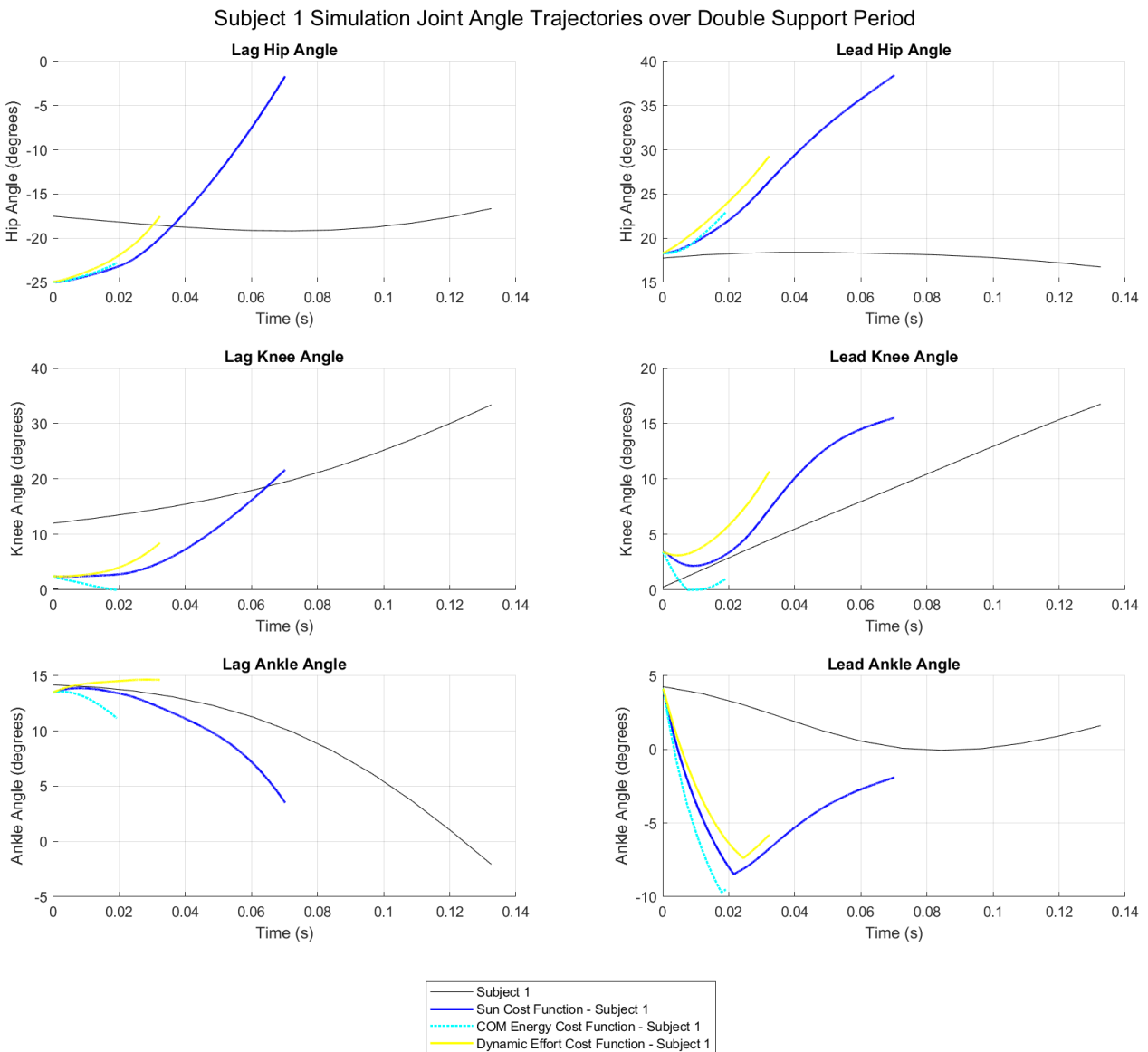
Figure 4.9: Subject 1 simulated sagittal plane joint angle trajectories for DS period with varying optimization targets.

subjects (1 and 2). However, consistent with simulated data for Subject 4, different cost functions result in varied solutions. This finding gives promise to the new optimization targets proposed in this work: work done on the COM and dynamic effort.

Simulated joint angle trajectories presented in Figures 4.8, 4.9, and 4.10, however, do not give significant information about the *quality* of simulation resulting from the application of new optimization targets. It is unreasonable to draw conclusions about simulation performance from

Subject 2 Simulation Joint Angle Trajectories over Double Support Period
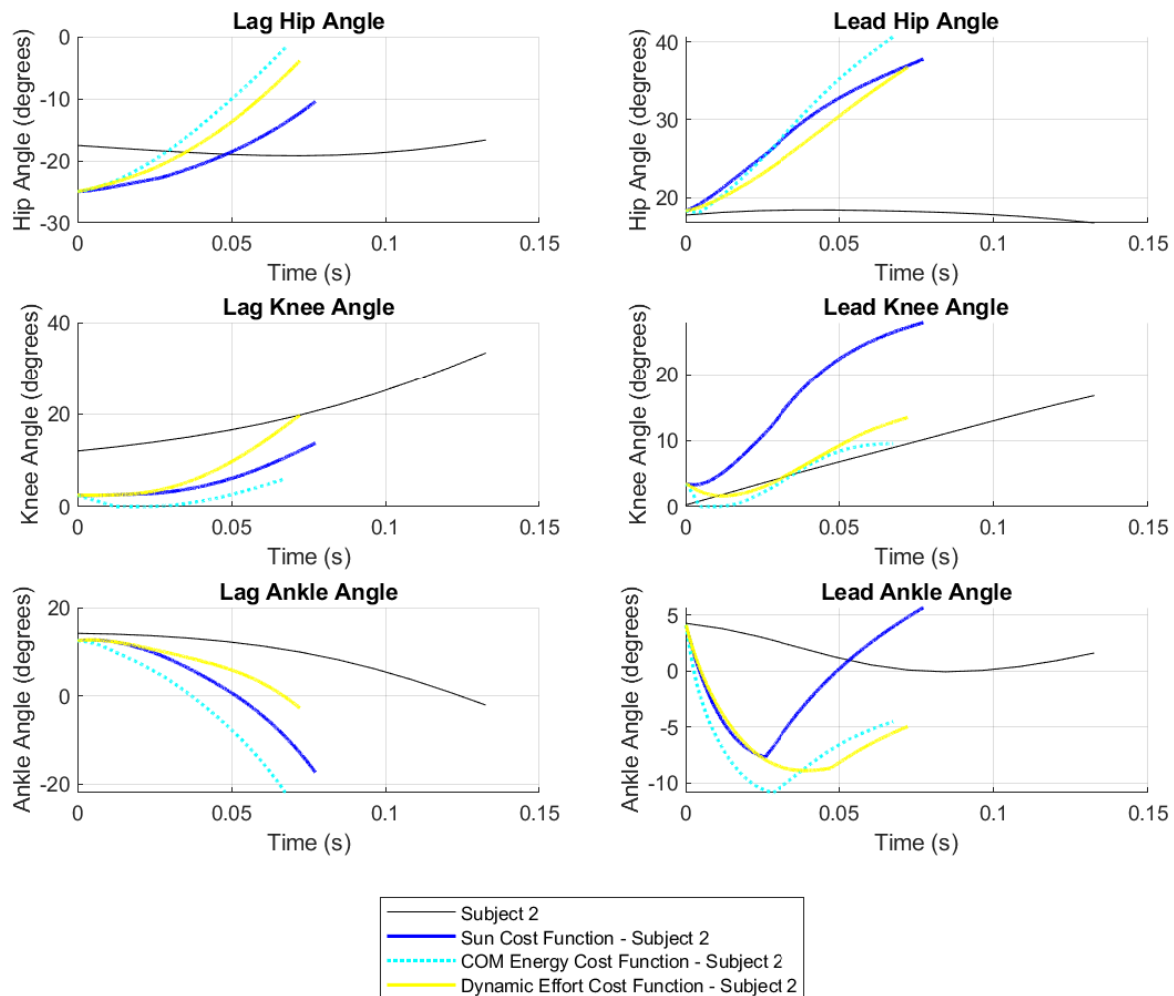
Figure 4.10: Subject 2 simulated sagittal plane joint angle trajectories for DS period with varying optimization targets.

such small window of the GC because it has been shown that the transitions between periods are extremely important in the simulation of human gait. Additionally, the required "manufacture" of IC sets, given that subject data did not provide IC sets compatible with the model GRF, again points to necessary model refinements before a complete evaluation of optimization targets can be made.

Though it is clear that there are challenges in the DS simulation framework to address, the current framework does demonstrate better control and predictive capability for DS than SS when

the given IC do not conflict with GRF. Future work is required to fully understand this dramatic difference, but it is likely that the optimization problem encountered in DS is of a different class than the SS optimization problem, which could be a result of the dynamic differences between an closed (DS) and open (SS) kinematic chain as discussed in Section 3.1. This exploration is outside the scope of this thesis, but the work presented here clearly demonstrates the dependence of MPC on successful optimization. Though in its current state, the simulation framework is not adequate for GC simulation, the successful application of new optimization targets within the framework in this thesis is promising for future success with the proposed framework, given appropriate optimization solution-finding methods are used.

CHAPTER 5

CONCLUSION AND FUTURE WORK

This thesis investigated the application of new optimization targets within an existing MPC framework [31], [32] to predictively simulate human walking patterns. Walking is one of the most routine human activities, but understanding of it is limited, and thus the application and development of gait-related treatments and devices is inhibited. In particular, development of active devices is limited especially by gait models lacking predictive capabilities. While a significant body of literature exists on gait modeling and optimization criteria to achieve simulated, normal gait, particularly with neuromuscular models, few studies have aimed to apply optimization targets which approximate metabolic cost to mechanical gait models. Even fewer have attempted this predictively, with no joint angle data specified *a priori*. The Sun model [31], [32] is one such mechanical framework which utilizes MPC to predict the dynamics of human walking. However, this simulation framework is limited to a half GC (assuming symmetry) and optimized only according to characteristic constraints.

In this thesis, the Sun framework and MPC control scheme [31], [32] were expanded to generate consecutive DS, SS, DS, and SS periods simulations. This GC simulation was not marked by TO and HS, but was C_0 continuous, which was not achieved by the Sun model [31], [32]. New cost functions were developed with energy-related optimization targets, dynamic effort and work done to the COM, which have been proposed as valid approximations of metabolic cost when musculature is not modeled [25], [7]. Though the inability of the model framework to generate a SS simulation that begins at TO prevented the application of new cost functions to simulation of a full GC, these optimization targets were successfully applied within the model framework for DS. It is important to note that the ability of optimization targets to generate normal walking patterns cannot be fully evaluated until a full GC can be generated. However, subject-specific joint trajectories from all simulations were compared with measured subject gait data, and initial observations about optimization target performance were made, consistent with clinical gait analysis methods.

This thesis has demonstrated that the MPC-based simulation framework, developed by Sun [31], [32] and expanded in this work, is not sufficient for the prediction of subject-specific gait in its current form. After failing to simulate a full GC by constraining the simulation to achieve consecutive DS, SS, DS, and SS periods, separate investigations of the effects of IC and joint

actuation during SS were conducted. Because no IC set resulted in successful simulation of SS, the failure of SS is likely not due to IC dependence. In addition, the joint actuation study demonstrated that resulting simulations during SS showed little to no MPC control action. This is likely due to limitations of the solution-finding methods used in the MPC framework. However, MPC could still be a viable method of gait prediction with alternative solution-finding methods, and the proposed framework with modifications to the optimization routine would be the most predictive gait simulation in the literature.

The framework proposed here is unique in that the final states and time of each period simulation are not constrained. Though many gait models recently developed claim to be predictive, nearly all specify joint positions at some point within the trajectory outside of the IC set. The gait model expanded in this work would fill a much-needed gap in gait modeling and simulation research because of its predictive nature. With the successful application of energy-related optimization targets in this thesis, the simulation framework proposed also unifies two major subdivisions of gait research: neuromuscular models which have identified measures that align with the goals of the CNS but are computationally expensive and mechanical models which capture the dynamics of gait but often lack control schemes which adequately model the delicate and predictive control of the CNS.

The application of energy-related optimization targets within MPC is a significant contribution to the simulation framework proposed by Sun [31], [32]. However, controller performance subject to new optimization targets, work done to the COM and dynamic effort, cannot be evaluated until a full GC simulation is achieved. Though this work does demonstrate that new optimization targets can be applied within the existing MPC simulation framework, more importantly this thesis identifies several limitations of the framework. The failure of the model to reliably meet characteristic constraints (which describe a GC marked by TO and HS), particularly in SS, prevents simulation of a full GC. The work in this thesis points primarily to the failure of the optimization routine within the MPC framework to reliably find a solution that meets constraints as the cause of this problem. If the optimization problem can be classified, an appropriate solution algorithm could be chosen which could reliably find a solution for any given set of constraints and IC. Identifying an appropriate solution algorithm could make the MPC framework proposed a viable method of gait prediction and simulation.

5.1 Future Work

MPC, by design, is an optimization-based predictive control method. Thus, controller performance can be limited by optimization performance. Dynamic models of human gait across literature, including the plant and internal models proposed by Sun, are large-DOF, non-linear dynamic systems which requires a optimization algorithm to navigate a complex solution space. Primarily, future work must characterize the optimization within the MPC framework to find an appropriate solution method.

To make the MPC framework a viable predictive simulation of human gait, a different solution method must be chosen. However, although the solution-finding method in SS is likely the most significant barrier to simulation of a full GC, this thesis identified several other areas for future work. With some characterization of the solution space, it is also possible that some other improvements to the model may improve the optimization performance of the framework.

Characteristic constraints may also need to be redefined in order to achieve repeatable transitions between period simulations. The difference between plant and internal model pairs for DS and SS periods, though seemingly necessary because of the dynamic differences between periods, does place significant emphasis on the transition between periods. Moving forward, it is possible that a "gain scheduling" approach be necessary, in which optimization targets change over the prediction horizon. This method could alleviate problems with period transitions by changing the target of the optimization routine to appropriate IC for the next period.

There are also a variety of ways in which the gait model could be improved, that may increase the frequency of finding an appropriate solution. In particular, the GRF and ankle-foot kinematic model should be redefined. The Sun model uses a combination of springs and dampers to model ground contact, but the value of these springs and dampers is not consistent between periods.

Additionally, the rigid, triangular shape of the foot may result in joint motion and torques that differ from that of normal ambulators. In normal walking ankle kinematics are of high importance, and the flexion of the foot may prove important. The dynamics of the foot have been modeled in a variety of ways across existing gait simulation literature, but the rounded ankle-foot model proposed by Ren [30] generated significantly improved ankle kinematics over the GC. Improvement of the fidelity of the foot and GRF model could actually improve the performance of the optimization by reducing the complexity of the solution space.

The simulation framework also remains reliant on base polynomial torque trajectories. These base polynomials, with passive spring and damping coefficients, should be optimized for a wider range of subjects so that the optimization initial guess is improved. With better control achieved through improving the optimization routine, an improved initial guess still improves the framework by reducing the time dedicated to optimization. Passive elements, like GRF models, should also be consistent across DS and SS models, since they are modeling dynamic elements of the same joints in each period.

Aside from improvements to the gait cycle, characteristic constraints of the simulation framework could be unified between periods by an empirical relationship between walking speed and step length. It has been shown that there is an optimal step-length for a given speed [41], so step length target could be calculated from self-selected walking speed. Thus, desired velocity would be the input for both objective functions.

Despite significant areas for future work, the significance of the simulation framework should not be overlooked. With the correction of SS period optimization, the MPC simulation framework proposed in this thesis is more predictive than any existing gait model in literature. MPC, though limited in its current application within this framework, remains a good candidate for the prediction and simulation of human gait. Further development of a predictive gait model would benefit a variety of fields. Trial and error processes currently in practice in the development of gait related treatments and devices could be eliminated with better understanding of normal gait and better tools to predict it.

REFERENCES

[1] Center for motion analysis. Medical College of Wisconsin.

[2] Orthopedic and rehabilitation engineering center. Marquette University.

[3] M. Ackerman and A. van den Bogert. Optimality principles for model-based prediction of human gait. *Journal of Biomechanics*, 43(6):1055–1060, April 2010.

[4] F.C. Anderson and M.G. Pandy. Dynamic optimization of human walking. *Journal of Biomechanical Engineering*, 123:381–390, October 2001.

[5] C. Azevedo, P. Poignet, and B. Espiau. Artificial locomotion control: From human to robots. *Robotics and Autonomous Systems*, 47(1):203–223, 2004.

[6] R. Baker. *Measuring Walking: A Handbook of Clinical Gait Analysis*. Mac Keith Press, London, 1st edition, 2013.

[7] R. Burdett, G. Skrinar, and S. Simon. Comparison of mechanical work and metabolic energy consumption during normal gait. *Journal of Orthopaedic Research*, 1(1):63–72, 1983.

[8] G. A. Cavagna, H. Thys, and A. Zamboni. The sources of external work in level walking and running. *Journal of Physiology*, (262):639–657, 1976.

[9] The Amputee Coalition. Limb loss statistics, 2019.

[10] P. Dempsey, R. Larsen, S. Parneet, J. Sacre, N. Straznicki, N. Cohen, E. Cerin, G. Lambert, N. Owen, B. Kingwell, and D. Dunstan. Benefits for type 2 diabetes of interrupting prolonged sitting with brief bouts of light walking or simple resistance activities. *Diabetes Care*, 39:964–972, 2016.

[11] J. Ding, C. Zhou, and X. Xiao. Energy-efficient bipedal gait pattern generation via com acceleration optimization. In *IEEE-RAS 18th International Conference on Humanoid Robots*. IEEE, November 2018.

[12] R. Fluit, M.M. van der Krogt, H. van der Kooij, N. Verdonschot, and H.F.J.M. Koopman. A simple controller for the prediction of three-dimensional gait. *Journal of Biomechanics*, 45:2610–2617, August 2012.

[13] S.R. Goldberg, S. Ounpuu, and S.L. Delp. The importance of swing-phase initial conditions in stiff-knee gait. *Journal of Biomechanics*, 36:1111–1116, March 2003.

[14] M. Hamer and Y. Chida. Walking and primary prevention: A meta-analysis of prospective cohort studies. *British Journal of Sports Medicine*, 42:238–243, November 2007.

[15] S. Hansen and A. Jones. Is there evidence that walking groups have health benefits? a systematic review and meta-analysis. *British Journal of Sports Medicine*, 49:710–715, January 2015.

[16] J.S. Higginson, R.R. Neptune, and F.C.Anderson. Simulated parallel annealing within a neighborhood for optimization of biomechanical systems. *Journal of Biomechanics*, 38:1938–1942, 2005.

[17] M. Karimian, F. Towhidkhah, and M. Rostami. Application of model predictive impedance control in analysis of human walking on rough terrains. *International Journal of Applied Electromagnetics and Mechanics*, 24:147–162, 2006.

[18] D. Katic and M. Vukobritovic. Survey of intelligent control techniques for humanoid robots. *Journal of Intelligent and Robotic Systems*, 37:117–141, 2003.

[19] Cynthia R. Lee and Claire T. Farley. Determinants of the center of mass trajectory in human walking and running. *Journal of Experimental Biology*, (201):2935–2944, 1998.

[20] M. Lilja and T. Oberg. Proper time for definitive transtibial prosthetic fitting. *Journal of Prosthetics and Orthotics*, 9(2):90–95, 1997.

[21] R. Marler and J. Arora. Survey of multi-objective optimization methods for engineering. *Journal of Structural Multidisciplinary Optimization*, 26(1):369–395, 2004.

[22] A.E. Martin and J.P. Schmiedeler. Predicting human walking gaits with a simple planar model. *Journal of Biomechanics*, 47:1416–1421, 2014.

[23] Mathworks. Constrained nonlinear optimization algorithms: fmincon interior point algorithm.

[24] D. Mena, J. M. Mansour, and S. R. Simon. Analysis and synthesis of human swing leg motion during gait and its clinical applications. *Journal of Biomechanics*, 14(12):823–832, 1981.

[25] A. Minetti and R. Alexander. A theory of metabolic costs for bipedal gaits. *Journal of Theoretical Biology*, pages 467–476, 1997.

[26] S. Mochon and T.A. McMahon. Ballistic walking. *Journal of Biomechanics*, 13:49–57, 1980.

[27] R. R. Neptune, F. E. Zajac, and S. A. Kautz. Muscle mechanical work requirements during normal walking: the energetic cost of raising the body's center of mass is significant. *Journal of Biomechanics*, 37:817–825, 2004.

[28] J. Perry and J.M. Burnfield. *Gait Analysis: Normal and Pathological Function*. Slack Incorporated, Thorofare, New Jersey, second edition, 2010.

[29] David C. Remy and Darryl G. Thelen. Optimal estimation of dynamically consistent kinematics and kinetics for forward dynamic simulation of gait. *Journal of Biomechanical Engineering*, 131, March 2009.

[30] L. Ren, R.K. Jones, and D. Howard. Predictive modeling of human walking over a complete gait cycle. *Journal of Biomechanics*, 2007.

[31] J. Sun. *Dynamic Modeling of Human Gait Using a Model Predictive Control Approach*. PhD thesis, Marquette University, Milwaukee, WI, May 2015.

[32] J. Sun, S. Wu, and P. Voglewede. Dynamic simulation of human gait model with predictive capability. *Journal of Biomechanical Engineering*, 140(3), 2018. 031008.

[33] H. Van der Kooij, R. Jacobs, B. Koopman, and F. Van der Helm. An alternative approach to synthesizing bipedal walking. *ASME Journal of Mechanical Design*, 129:595–601, June 2007.

[34] N. Van der Noot, Auke J. Ijspeert, and R. Ronsse. Biped gait controller for large speed variations, combining reflexes and a central pattern generator in a neuromuscular model. In *2015 IEEE International Conference on Robotics and Automation (ICRA)*. IEEE, May 2015.

[35] B.W. Verdaasdonk, H.F.J.M. Koopman, and F.C.T. van der Helm. Energy efficient walking with central pattern generators: From passive dynamic walking to biologically inspired control. *Journal of Biological Cybernetics*, pages 49–61, 2009.

[36] L. Wang. *Model Predictive Control System Design and Implementation Using MATLAB*. London: Springer, 2009.

[37] M. Wang, R. Wang, J. Zhao, and P. Sun. An optimized algorithm based on energy efficiency for gait planning of humanoid robots. In *44th Annual Conference of the IEEE Industrial Electronics Society*. IEEE, October 2018.

[38] E.R. Westerverlt, J.W. Grizzle, and D.E. Koditschek. Hybrid zero dynamics of planar biped walkers. *IEEE Transactions on Automatic Control*, 48(1):42–56, 2003.

[39] D.A. Winter. *Biomechanics and Motor Control of Human Gait*. Wiley, Ontario, Canada, fifth edition, 2009.

[40] Y. Xiang, J. Arora, and K. Abdel-Malek. Physics-based modeling and simulation of human walking. *Journal of Structural and Multidisciplinary Optimization*, 42(1):1–23, July 2010.

[41] M. Y. Zarrugh, F. N. Todd, and H. J. Ralston. Optimization of energy expenditure during level walking. *European Journal of Applied Physiology*, 33:293–306, 1974.

[42] X. Zhang and Z. Mingguo. Humanoid robot gait planning based on virtual supporting point. In *IEEE International Conference on Robotics and Biomimetics*. IEEE, December 2018.

[43] K. Ziegler-Graham, E. MacKenzie, P. Ephraim, T. Travison, and R. Brookmeyer. Estimating the prevalence of limb loss in the united states: 2005-2050. *American Congress of Rehabilitation Medicine and the American Academy of Physical Medicine and Rehabilitation*, 89:422–429, March 2008.

APPENDIX A

USE OF LAGUERRE FUNCTIONS IN DISCRETE MODEL PREDICTIVE CONTROL

A.1 Laguerre Functions

This Appendix describes the derivation and development of both continuous and discrete Laguerre functions. As described in Section , Laguerre functions are a set of orthonormal basis functions used to parameterize the control inputs of the MPC framework proposed in this thesis.

Within the Discrete MPC (DMPC) framework applied, the goal is to optimize the future control trajectory, $\Delta\mathbf{u}(k)$ according to a cost function. However, because of the non-linear, large DOF internal models, introducing a set of orthonormal basis functions allows a simpler solution and faster optimization. For simplicity, Laguerre functions as orthonormal basis functions will be introduced in continuous time, before being applied to the discrete controller.

Given a set of functions, $l_i(t), i = 1, 2, 3, ...$, orthonormal and complete over the interval $[0, \infty)$, an arbitrary function $f(t)$ has a formal expansion analagous to a Fourier Expansion,

$$f(t) \approx \sum_{i=1}^{N} c_i l_i(t) \ , \tag{A.1}$$

where c_i are coefficients that can be determined optimally [36].

Laguerre Functions [1] are one such set of functions, orthonormal and complete for any $p > 0$, and are given:

$$l_1(t) = \sqrt{2p}e^{-pt} \tag{A.2}$$

$$l_2(t) = \sqrt{2p}(-2pt + 1)e^{-pt}$$

$$\vdots$$

$$l_i(t) = \sqrt{2p}\frac{e^{-pt}}{(i-1)!}\frac{d^{i-1}}{dt^{i-1}}[t^{i-1}e^{-2pt}] \ ,$$

where p is the scaling factor which determines the exponential decay rate [36] (note that p is different from the vector, $\mathbf{p}$, used in the main body of this thesis which represents the array of control inputs).

---

[1]Because of the derivative term in the formulation, some texts denote these formulas Laguerre *polynomials* when $i \in \mathbb{N}$ and Laguerre *functions* when $i \in \mathbb{R} \setminus \mathbb{N}$. This paper will use Laguerre functions as a general descriptor of the set of orthonormal and complete functions where $i \in \mathbb{R}$.

A.1.1 Laguerre Functions in MPC

Laguerre functions are particularly useful for use in parameterizing functions within state space systems because of their simple Laplace transforms, allowing for a systematic method to generate functions through a state space Laguerre network[2].

Two parameters, M and p characterize the Laguerre function approximation in continuous time. M, the number of Laguerre functions used and therefore the number of coefficients to be optimized, should be selected based on the order of the expected control trajectory. The scaling factor, p, is analogous to the control window when applied to MPC, since it determines the decay rate of the Laguerre functions. A larger p corresponds to a longer control window, N_c, but is more computationally intensive.

In continuous time for a single-input, single-output (SISO) system, the control vector which is optimized is given as a function of time, $u(t)$.

Taking the state vector,

$$\mathbf{L}(t) = \begin{bmatrix} l_1(t) & l_2(t) & ... & l_M(t) \end{bmatrix}^T ,$$

where l_i is the inverse Laplace transform of the ith filter in the frequency-domain Laguerre network, and the initial conditions of the state vector to be

$$\mathbf{L}(0) = \sqrt{2p} \begin{bmatrix} 1 & 1 & ... & 1 \end{bmatrix}^T ,$$

then the Laguerre functions satisfy the state space equation [36]:

$$\begin{bmatrix} \dot{l}_1 \\ \dot{l}_2 \\ \vdots \\ \dot{l}_M \end{bmatrix} = \begin{bmatrix} -p & & ... & 0 \\ -2p & -p & ... & 0 \\ \vdots & \ddots & \ddots & \vdots \\ -2p & -2p & ... & -p \end{bmatrix} \begin{bmatrix} l_1(t) \\ l_2(t) \\ \vdots \\ l_M(t) \end{bmatrix} . \tag{A.3}$$

Thus,

$$\mathbf{L}(t) = e^{A_p t} \mathbf{L}(0) , \tag{A.4}$$

---

[2]Here, a Laguerre Network refers to a series of Laguerre Filters, which are no more than the Laplace transform of the Laguerre functions defined above. For more information on this process and derivation, see [36]

where

$$A_p = \begin{bmatrix} -p & & \cdots & 0 \\ -2p & -p & \cdots & 0 \\ \vdots & \ddots & \ddots & \vdots \\ -2p & -2p & \cdots & -p \end{bmatrix} .$$

This final form gives the Laguerre functions of order 1 through M for all t as a function of the scaling factor, p.

This simple solution can be used to parameterize an arbitrary continuous trajectory shown in Equation A.1, by using an optimization routine to identify the coefficients that allow for the closest approximation.

A.1.2 Laguerre Functions in DMPC

By identifying a discrete formulation it is also possible to use Laguerre functions to parameterize the control trajectory in DMPC, using a derivation similar to that demonstrated in continuous time.

In discrete time for a single-input, single-output (SISO) system, the control vector which is optimized is

$$\Delta \mathbf{U} = \begin{bmatrix} \Delta u(k_i) & \Delta u(k_i + 1) & \cdots & \Delta u(k_i + N_C - 1) \end{bmatrix}^T .$$

From this, the control signal at each time, k_i, can be separated using the Dirac Delta function, δ, or pulse operator, which shifts the control action forward [36]:

$$\Delta \mathbf{u}(k_i + i) = \begin{bmatrix} \delta(i) & \delta(i-1) & \cdots & \delta(i + N_C - 1) \end{bmatrix} .$$

Approximating this discrete trajectory requires discrete Laguerre network, which can be achieved by a discretization of a continuous-time Laguerre network. Taking the inverse z-transform of the discrete Laguerre network gives the discrete expression of the Laguerre functions, which can be expressed in vector form:

$$\mathbf{L}(k) = \begin{bmatrix} l_1(k) & l_2(k) & \cdots & l_M(k) \end{bmatrix}^T ,$$

where $l_i(k)$ is the i'th discrete laguerre function expression.

Table A.1: Joint Control for SS and DS Periods.

Period	Controller	Joint Angle
SS	MPC	stance ankle, swing ankle, swing knee, swing hip
	PID	stance knee, stance hip
DS	MPC	stance ankle, stance knee, swing ankle, swing knee
	PID	stance hip, swing hip

This set of functions satisfies the difference equation [36],

$$\begin{bmatrix} l_1(k+1) \\ l_2(k+1) \\ l_3(k+1) \\ l_4(k+1) \\ l_5(k+1) \\ l_6(k+1) \end{bmatrix} = \begin{bmatrix} a & 0 & 0 & 0 & 0 & 0 \\ \beta & a & 0 & 0 & 0 & 0 \\ -a\beta & \beta & a & 0 & 0 & 0 \\ a^2\beta & -a\beta & \beta & a & 0 & 0 \\ -a^3\beta & a^2\beta & -a\beta & \beta & a & 0 \\ a^4\beta & -a^3\beta & a^2\beta & -a\beta & \beta & a \end{bmatrix} \begin{bmatrix} l_1(k) \\ l_2(k) \\ l_3(k) \\ l_4(k) \\ l_5(k) \\ l_6(k) \end{bmatrix}, \tag{A.5}$$

where a is the discrete scaling factor, and $\beta = (1 - a^2)$, for M = 6. With the initial conditions vector,

$$\mathbf{L}(0) = \sqrt{\beta} \begin{bmatrix} 1 & -a & a^2 & -a^3 & a^4 & -a^5 \end{bmatrix}^T ,$$

each Laguerre function is given for all k by the difference equation (Equation A.5) as a function of the only the scaling factor.

Degree and Scaling Factor Selection

Selection of the degree, M, and scaling factor, a, affect the both the quality and computational intensity of the Laguerre function approximation. The effect of these parameters on the approximation is illustrated in Figure A.1, where Laguerre functions are used to parameterize the impulse response of an arbitrary system. Increasing the degree of the approximation or scaling factor both increase the computational intensity of the solution, but will achieve better results. For that reason, in a controller application, each should be selected as the minimum acceptable value.

A.2   Controller Application

Within the gait simulation framework, internal models are used to optimize joint moments of four joints during each period (Figure 2.4), single support (SS) and double support (DS), and the remaining two are controlled by auxiliary PID controllers to reduce the
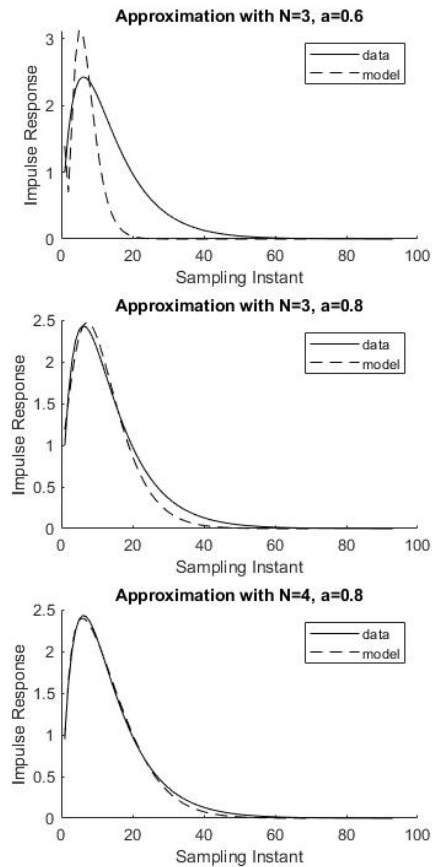
Figure A.1: Laguerre function approximation of an arbitrary impulse response.

computational load (Table A.1). Laguerre functions ($M = 6$, $a = 0$.) are used to parameterize the control trajectory within each joint controlled by MPC. These moments are then saved to be applied to the full plant model.

MPC requires finding of an optimal control input solution which meets target gait descriptors, such as step length or walking speed, repeatedly. The optimization scheme by which this solution is found is flexible. This simulation framework uses a nonlinear programming solver within MATLAB to find the minimum of a constrained, nonlinear, multivariable function.

To increase the speed of optimization convergence, the Laguerre function approximation acts in conjunction with a base polynomial, $f(u)$, where u is the simulation time. These base polynomials set the initial guess of the optimization to be a curve-fit trajectory of subject-specific torque data acquired during gait analysis. Figure A.2 shows this formulation within an
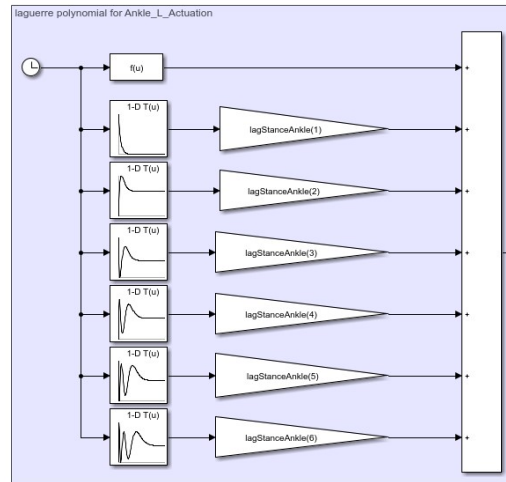
Figure A.2: Laguerre function application within a MPC-controlled joint actuator.

MPC-actuated joint in the model. The lookup tables contain the pre-calculated Laguerre functions over the prediction horizon, and each Laguerre function value is multiplied by it's respective optimized coefficient, before being added to the base polynomial.

Laguerre functions are a useful addition to an MPC system to simplify the extremely complex solution space. Further development of a predictive gait model would benefit a variety of fields. Trial and error processes currently in practice in the development of gait related treatments and devices could be eliminated with better understanding of normal gait and better tools to predict it.

A.3   MATLAB Code for Discrete Laguerre Function Generation

MATLAB code to generate figure which illustrates the effect of the degree, M, and scaling factor, a, on both the quality and computational intensity of the Laguerre function approximation for the impulse response of an arbitrary system.

```
1  %% Generate Laguerre function Impulse Approximation Example
2  clc, clear all, close all
3  %%
4  numd = [1 -0.1];
5  dend = conv([1 -0.8],[1 -0.9]);
6  H = impz(numd,dend);
7  %% approx a
```

```
 8  a = 0.6;
 9  N = 3;
10  %define laguerre functions
11  beta = 1 - a.^2;
12  A_l = [a 0 0; beta a 0; -a*beta beta a];
13  L_0 = sqrt(beta)*[1; -a; a^2];
14  k_end = 69;
15  k = 1:k_end+1
16  L(1,:) = L_0;
17  for i = 1:k_end
18  L(i+1,:) = A_l*L(i,:)';
19  end
20  %find coefficients for approximation
21  c = zeros(1,N);
22  for i = 1:N
23  for ii = 1:k_end
24  c(i) = H(ii)*L(ii,i)+c(i);
25  end
26  end
27  %approximate solution
28  H_model_a = zeros(1,N);
29  for i = 1:N
30  H_model_a = c(i)*L(:,i) + H_model_a;
31  end
32  %% approx b
33  clear L
34  a = 0.8;
35  N = 3;
36  %define laguerre functions
37  beta = 1 - a.^2;
38  A_l = [a 0 0; beta a 0; -a*beta beta a];
39  L_0 = sqrt(beta)*[1; -a; a^2];
40  k_end = 69;
41  k = 1:k_end+1;
42  L(1,:) = L_0;
43  for i = 1:k_end
44  L(i+1,:) = A_l*L(i,:)';
45  end
46  %find coefficients for approximation
47  c = zeros(1,N);
```

```matlab
48  for i = 1:N
49  for ii = 1:k_end
50  c(i) = H(ii)*L(ii,i)+c(i);
51  end
52  end
53  %approximate solution
54  H_model_b = zeros(1,N);
55  for i = 1:N
56  H_model_b = c(i)*L(:,i) + H_model_b;
57  end
58  %% approx c
59  clear L
60  a = 0.8;
61  N = 4;
62  %define laguerre functions
63  beta = 1 - a.^2;
64  A_l = [a 0 0 0; beta a 0 0; -a*beta beta a 0; a^2*beta -a*beta  beta a];
65  L_0 = sqrt(beta)*[1; -a; a^2; -a^3];
66  k_end = 69;
67  k = 1:k_end+1;
68  L(1,:) = L_0;
69  for i = 1:k_end
70  L(i+1,:) = A_l*L(i,:)';
71  end
72  %find coefficients for approximation
73  c = zeros(1,N);
74  for i = 1:N
75  for ii = 1:k_end
76  c(i) = H(ii)*L(ii,i)+c(i);
77  end
78  end
79  %approximate solution
80  H_model_c = zeros(1,N);
81  for i = 1:N
82  H_model_c = c(i)*L(:,i) + H_model_c;
83  end
84  %% plot results
85  figure (1)
86  subplot(311)
87  hold on
```

```
88   plot(H,'k-')
89   plot(k,H_model_a,'k--')
90   legend('data','model')
91   xlabel('Sampling Instant')
92   ylabel('Impulse Response')
93   title('Approximation with N=3, a=0.6')
94   subplot(312)
95   hold on
96   plot(H,'k-')
97   plot(k,H_model_b,'k--')
98   legend('data','model')
99   xlabel('Sampling Instant')
100  ylabel('Impulse Response')
101  title('Approximation with N=3, a=0.8')
102  subplot(313)
103  hold on
104  plot(H,'k-')
105  plot(k,H_model_c,'k--')
106  legend('data','model')
107  xlabel('Sampling Instant')
108  ylabel('Impulse Response')
109  title('Approximation with N=4, a=0.8')
110  % figure(2)
111  % plot(k,L)
112  % legend('1','2','3','4')
```

A.4   MATLAB Code for Discrete Laguerre Polynomial Development

This MATLAB code generates the Laguerre functions ($M = 6, a = 0.$) used to parameterize the control trajectory within each joint controlled by MPC and the base polynomials, $f(u)$, where u is the simulation time. These base polynomials set the initial guess of the optimization to be a curve-fit trajectory of subject-specific torque data acquired during gait analysis.

```
1   %% Laguerre Polynomial Development
2   %find polyfit constants to give best initial guess from Winter2009 norm data
3   clc, clear all, close all
4   %% Single Support Period
```

```matlab
5   %% generate polynomial fit data for normal ambulator
6   %add winters data
7   filename = 'C:\Users\jess-local\OneDrive - Marquette University\Research\Normal ...
        Gait Data\Winters Gait Data.xlsx';
8   trajec.ss(:,1) = xlsread(filename,'M29:M56'); %stance ankle (13 timesteps after ...
        RHS - 27 timesteps later)
9   trajec.ss(:,2) = xlsread(filename,'M2:M29'); %swing ankle (RTO - RHS)
10  trajec.ss(:,3) = xlsread(filename,'N2:N29'); %swing knee (RTO - RHS)
11  trajec.ss(:,4) = xlsread(filename,'O2:O29'); %swing hip  (RTO - RHS)
12  trajec.sstime = xlsread(filename,'C2:C29'); %time   (RTO - RHS)
13  %add polyfit data
14  %the polyfits act as a baseline trajectory from which the laguerre function
15  %formulation deviates, they should be a close approximation of winters data
16  x = 0:0.01:(trajec.sstime(end)+0.02);
17  lag.ss.polyfit1 = polyfit(trajec.sstime,trajec.ss(:,1),5);
18  lag.ss.p1 = polyval(lag.ss.polyfit1,x);
19  lag.ss.polyfit2 = polyfit(trajec.sstime,trajec.ss(:,2),8);
20  lag.ss.p2 = polyval(lag.ss.polyfit2,x);
21  lag.ss.polyfit3 = polyfit(trajec.sstime,trajec.ss(:,3),8);
22  lag.ss.p3 = polyval(lag.ss.polyfit3,x);
23  lag.ss.polyfit4 = polyfit(trajec.sstime,trajec.ss(:,4),8);
24  lag.ss.p4 = polyval(lag.ss.polyfit4,x);
25  %plot data and laguerre polyfit constants curve-fits
26  for i = 1:4
27  subplot(str2num(['41' num2str(i)]))
28  hold on
29  p = eval(['lag.ss.p' num2str(i)]);
30  plot(trajec.sstime,trajec.ss(:,i),'.',x,p) %,x,sun.ss.fit(:,i)
31  end
32  %% generate discrete laguerre functions
33  %formulation from Wang2009, utilizing a discrete laguerre network state-space ...
        representation
34  a = 0.8;
35  beta = 1 - a.^2;
36  A_l = [a 0 0 0 0 0; beta a 0 0 0 0; -a*beta beta a 0 0 0;...
37  a^2*beta -a*beta  beta a 0 0; -a^3*beta a^2*beta -a*beta beta a 0;...
38  a^4*beta -a^3*beta a^2*beta -a*beta beta a];
39  L_0 = sqrt(beta)*[1; -a; a^2; -a^3; a^4; -a^5];
40  t_end = 0.500;
41  dt = 0.005;
```

```matlab
42  t = 0:dt:t_end;
43  k_end = t_end/dt;
44  L(1,:) = L_0;
45  for k = 1:k_end
46  L(k+1,:) = A_l*L(k,:)';
47  end
48  figure(2)
49  plot(t,L)
50  legend('l_1','l_2','l_3','l_4','l_5','l_6')
51  ylabel('Amplitude')
52  xlabel('Sampling Instant, k')
53  title('Laguerre Functions, M=6, a=0.8')
54  grid on
```

APPENDIX B

SUBJECT ANTHROPOMETRIC DATA AND GAIT REPORTS

This appendix contains the measured subject anthropometry and processed motion capture data collected and used in this thesis. The motion capture protocol used for Subjects 1 and 2 is presented in Section 3.4. Subject 4 motion capture was conducted by Sun [31]. Table B.1 summarizes the collection methods of data presented here.

Table B.1: Description of subject data used.

	Subject 1	**Subject 2**	**Subject 4**
Collected by	Author	Author	Sun [31]
Collected at	OREC Gait Lab [2]	OREC Gait Lab [2]	MCW CMA [1]
Motion Capture System	Qualisys	Qualisys	Vicon
Data Processing	Visual3D	Visual3D	Unknown
Kinematic Data	Yes	Yes	Yes
Kinetic Data	Invalid*	Yes	Unknown

*Force plate data was not collected.

Anthropometric measurements made for each subject include height, weight, orthosis mass, and bilateral limb length and circumference, summarized in Table B.2.

Table B.2: Description of anthropometric measurements.

Measurement	**Landmark Description of Measurement**
Inter ASIS Distance	distance from left and right anterior superior iliac spine (ASIS)
Leg Length	distance from ASIS to lateral malleoli
Thigh Length	distance from greater trochanter to lateral femoral epicondyle
Knee Diameter	distance from medial to lateral femoral epicondyle
Ankle Diameter	distance from medial to lateral malleoli
Thigh Proximal Circumference	circumference just distal to ischial tuberosity
Thigh Distal Circumference	circumference just proximal to the patella
Foot Length*	distance from calcaneal tuberosity to distal end of hallux
Foot Width*	distance from first metatarsal head to fifth metatarsal head
Foot Rocker*	distance from calcaneal tuberosity to first metatarsal head

*Measurement made on AFO instead of subject

Subject anthropometry is converted to model parameters with the following MATLAB script, which is shown for Subject 2 parameter generation:

```matlab
1  %% Patient Data Model Creation
2  %allows input of subject parameters to generate .mat file
3
4  %% model name and subject id
5  %  ***EDIT THESE PARAMETERS ONLY***
6  id = 02;
7  param.name = ['SubjectID_',num2str(id)];
8  param.note = 'Thayer Subject 2, 2019';
9
10 %input anthropometric measurements
11 param.gender = 'female';
12 param.age = '38';
13 param.height = 1.78; % (m)
14 param.weight = 78.02; % (kg)
15 param.orthosisWeight = 1; % (kg)
16 param.legLength = 1.01; %ASIS to lateral malleoli (m)
17 param.thighLength = 0.60; %greater trochanter to lateral femoral epicondyle (m)
18 param.kneeDiam = 0.1165; %knee diameter (m)
19 param.ankleDiam = 0.07; %ankle diameter (m)
20 param.interASIS = 0.32; %ASIS to ASIS (m)
21 param.thighProx = 0.66; %thigh proximal circumference (m)
22 param.thighDist = 0.45; %thigh distal circumference (m)
23 param.malHeight = 0.07; %height of malleolus\ankle joint from ground (m)
24 param.footLength = 0.25; %length of foot, measured from AFO (m)
25 param.rockerLength = 0.185; %length from heel to ball of foot, measured from AFO (m)
26 param.footWidth = 0.10; %width of ball of foot, measured from AFO (m)
27
28 %% create simulation parameters
29 param.var(1) = "bodymass"; param.val(1) = param.weight;
30 param.var(2) = "F_C"; param.val(2) = 0.33*param.rockerLength;
31 param.var(3) = "F_H"; param.val(3) = param.malHeight;
32 param.var(4) = "F_L"; param.val(4) = param.rockerLength;
33 param.var(5) = "F_M"; param.val(5) = 0.0145*param.val(1);
34 param.var(6) = "F_I"; param.val(6) = param.val(5)*(0.475*param.val(3))^2;
35 param.var(7) = "F_W"; param.val(7) = param.footWidth;
36 param.var(8) = "S_L"; param.val(8) = param.legLength - param.thighLength;
37 param.var(9) = "S_R1"; param.val(9) = param.ankleDiam/2;
38 param.var(10) = "S_R2"; param.val(10) = param.thighDist/(2*pi);
39 param.var(11) = "S_M"; param.val(11) = 0.0465*param.weight;
```

```
40  param.var(12) = "S_I"; param.val(12) = param.val(11)*(0.302*param.val(8))^2;

41  param.var(13) = "T_L"; param.val(13) = param.thighLength;

42  param.var(14) = "T_R1"; param.val(14) = param.thighDist/(2*pi);

43  param.var(15) = "T_R2"; param.val(15) = param.thighProx/(2*pi);

44  param.var(16) = "T_M"; param.val(16) = 0.100*param.val(1);

45  param.var(17) = "T_I"; param.val(17) = param.val(16)*(0.475*param.val(13))^2;

46  param.var(18) = "HAT_L"; param.val(18) = (0.818-0.530)*param.height;

47  param.var(19) = "HAT_M"; param.val(19) = 0.678*param.val(1);

48  param.var(20) = "HAT_I"; param.val(20) = param.val(19)*(0.496*param.val(18))^2;

49  param.var(21) = "HAT_a"; param.val(21) = 0.2;

50  param.var(22) = "HAT_b"; param.val(22) = 0.11;

51

52  %% save to .mat file to be opened and applied in main script

53  save(['Param_Subject_',num2str(id)],'param');
```

B.1 Anthropometry

Table B.3: Subject anthropometric measurements.

Measurement	Subject 1	Subject 2	Subject 4
Age	26	38	28
Sex	Male	Female	Male
Height	1.83 m	1.78 m	1.91 m
Weight	85.7 kg	78.0 kg	86.2 kg
Inter ASIS Distance	0.30 m	0.32 m	0.26
Leg Length	0.81 m	1.01 m	1.03 m
Thigh Length	0.40 m	0.60 m	N/A
Knee Diameter	0.10 m	0.12 m	0.10 m
Ankle Diameter	0.067 m	0.07 m	0.08 m
Thigh Proximal Circumference	0.63 m	0.66 m	N/A
Thigh Distal Circumference	0.43 m	0.45 m	N/A
Foot Length*	0.27 m	0.25 m	N/A
Foot Width*	0.09 m	0.10 m	N/A
Foot Rocker*	0.20 m	0.19 m	N/A

*Measurement made on AFO instead of subject

B.2 Subject 1 Normal Ambulation Gait Report
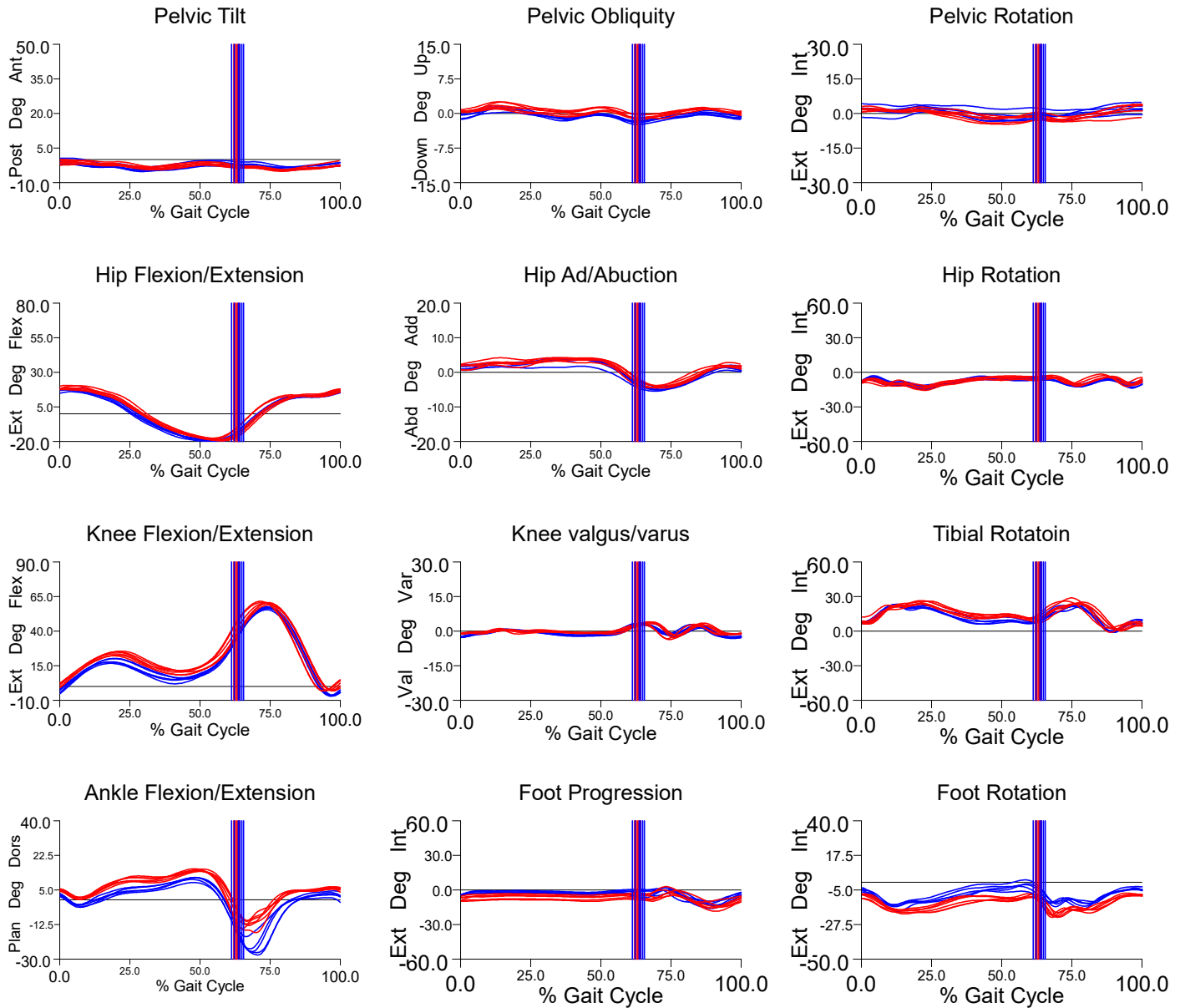
Kinematics and Temporal Parameters

	Pelvic Tilt	Pelvic Obliquity	Pelvic Rotation
Hip Flexion/Extension	Hip Ad/Abuction	Hip Rotation	
Knee Flexion/Extension	Knee valgus/varus	Tibial Rotatoin	
Ankle Flexion/Extension	Foot Progression	Foot Rotation	

Speed	1.21 m/s	0.66 Statures/s
Stride	Wid(12) 0.12±0.02m	Len(12) 1.46±0.03m
Cycle Time	Computed: 1.20 s	Actual (12) 1.21±0.02 s
	Measure±StdDev (Count)	Measure±StdDev (Count)
Stance Time	Left : 0.76±0.01 s (5)	Right : 0.77±0.01 s (6)
Swing Time	Left : 0.44±0.02 s (8)	Right : 0.44±0.03 s (9)
Cycle Time	Left : 1.21±0.02 s (6)	Right : 1.21±0.03 s (6)
Strides / Minute	Left : 49.47±0.97 (6)	Right : 49.79±1.08 (6)

Dbl Limb Support (17)   **0.32±0.04 s**

Kinetic Parameters
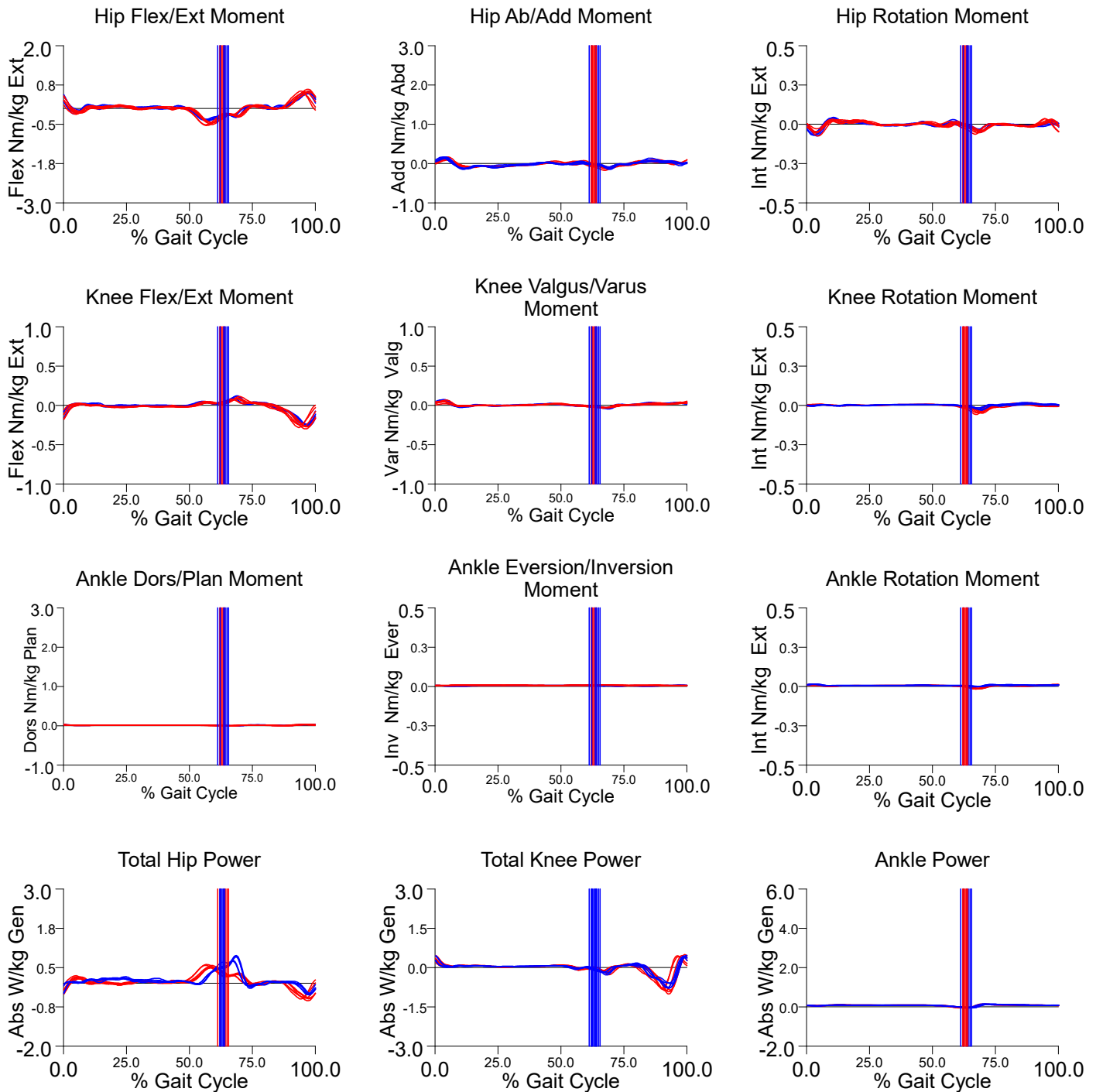
Hip Flex/Ext Moment

Hip Ab/Add Moment

Hip Rotation Moment

Knee Flex/Ext Moment

Knee Valgus/Varus Moment

Knee Rotation Moment

Ankle Dors/Plan Moment

Ankle Eversion/Inversion Moment

Ankle Rotation Moment

Total Hip Power

Total Knee Power

Ankle Power

Adult Normal Subjects Information

Temporal Stride Parameters:
Walking Speed (m/s): Avg- 1.155 , SD- 0.142
Stride Length (m): Avg- 1.295 , SD- 0.098
Cadence (step/min)- Avg- 53.548 , SD- 5.842

Male: 5 , Female: 3
Left: 7 , Right: 7
Height (m): Avg- 1.73 , SD- 0.075
Weight (kg): Avg- 72.1 , SD- 12.887
Age: Avg- 22 , SD- 1.323

B.3 Subject 1 Rigid-Ankle Ambulation Gait Report
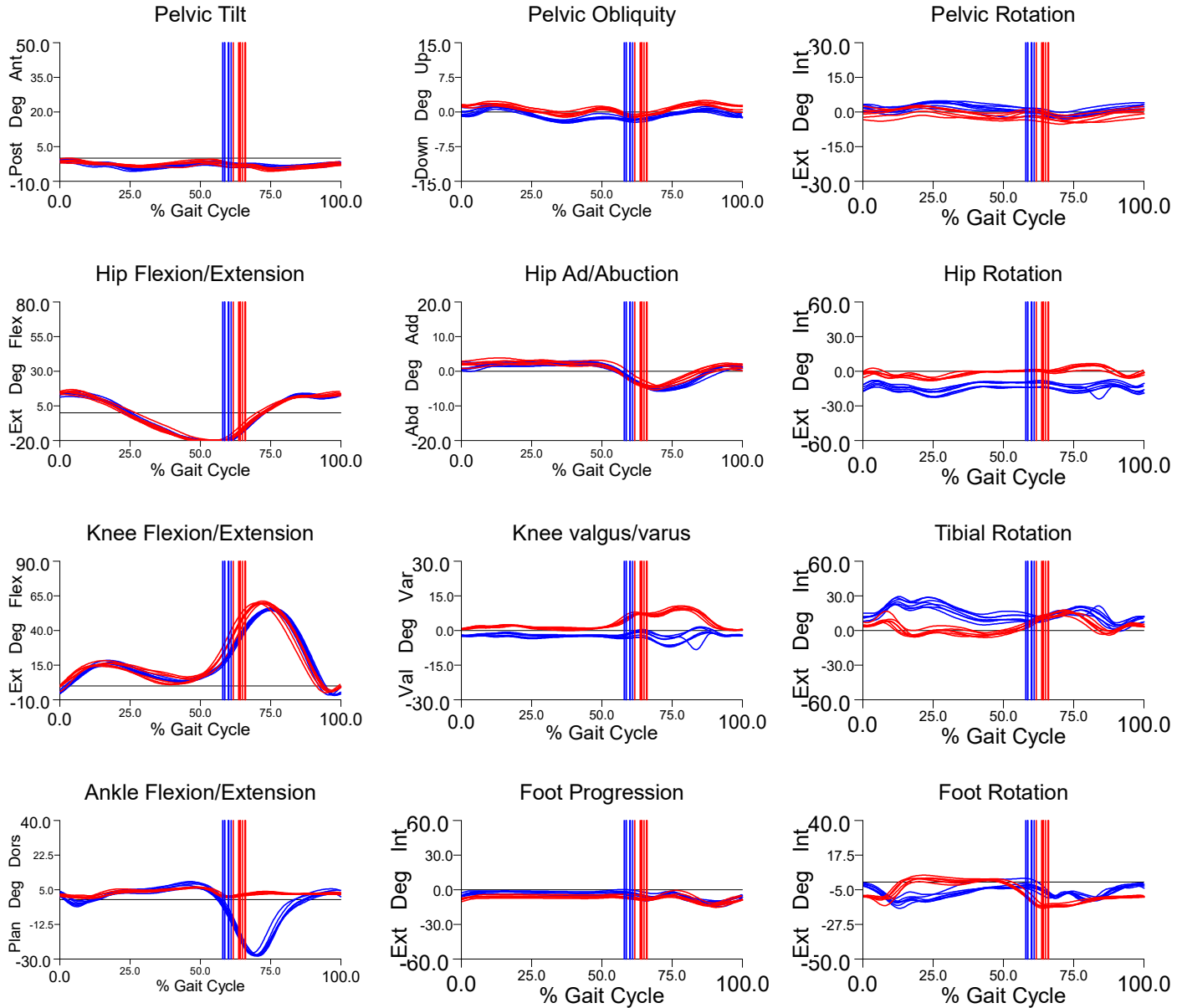
Kinematics and Temporal Parameters

Pelvic Tilt

Pelvic Obliquity

Pelvic Rotation

Hip Flexion/Extension

Hip Ad/Abuction

Hip Rotation

Knee Flexion/Extension

Knee valgus/varus

Tibial Rotation

Ankle Flexion/Extension

Foot Progression

Foot Rotation

Speed	1.14 m/s		0.62 Statures/s
Stride	Wid(13) 0.14±0.01m		Len(13) 1.38±0.03m
Cycle Time	Computed: 1.21 s		Actual (13) 1.21±0.02 s
	Measure±StdDev (Count)		Measure±StdDev (Count)
Stance Time	Left : 0.78±0.02 s (7)		Right : 0.72±0.01 s (7)
Swing Time	Left : 0.43±0.02 s (10)		Right : 0.49±0.01 s (9)
Cycle Time	Left : 1.21±0.02 s (7)		Right : 1.22±0.02 s (6)
Strides / Minute	Left : 49.77±0.92 (7)		Right : 49.24±0.63 (6)

Dbl Limb Support (20)   **0.29±0.05 s**

Kinetic Parameters
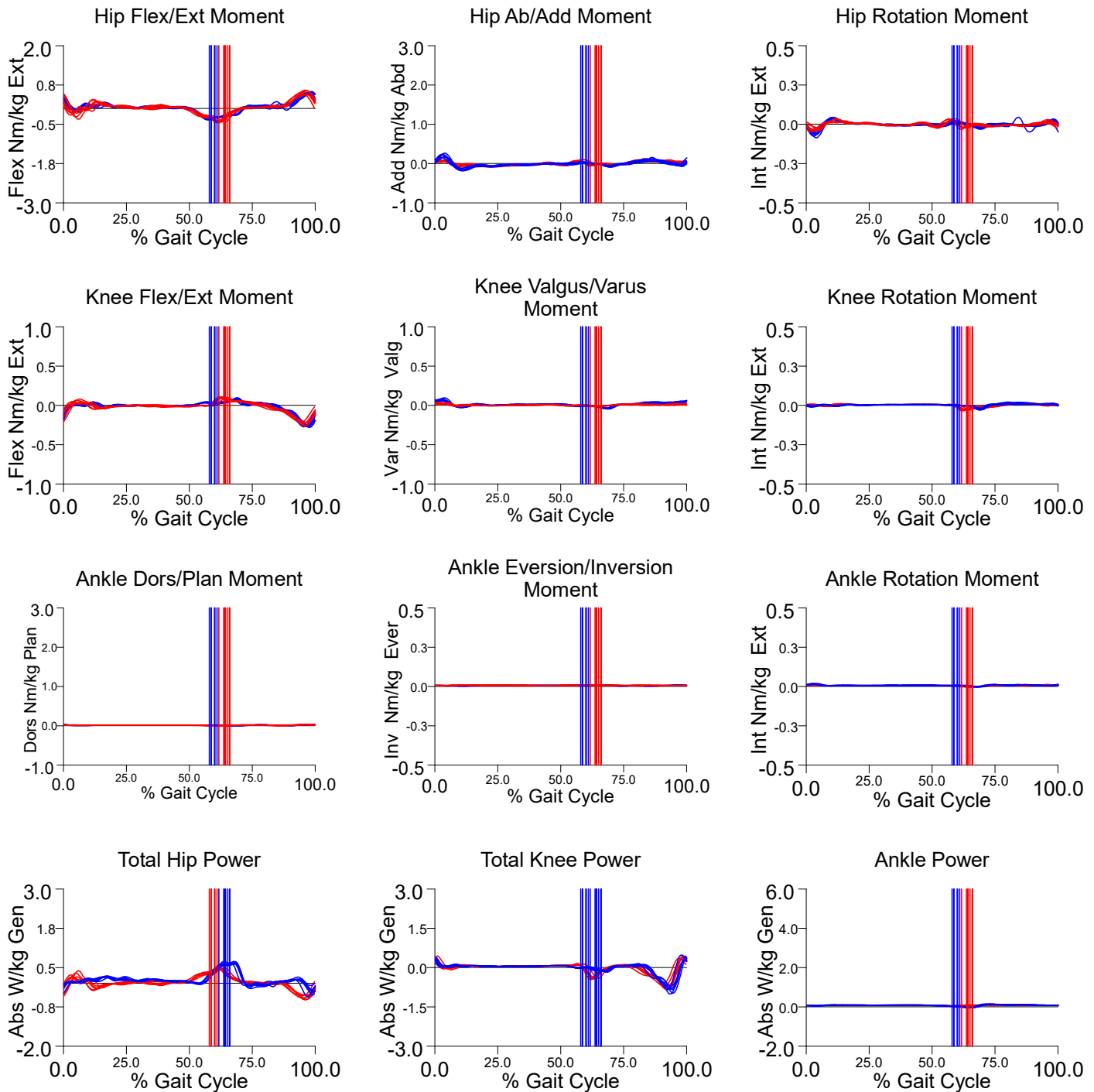
Hip Flex/Ext Moment

Hip Ab/Add Moment

Hip Rotation Moment

Knee Flex/Ext Moment

Knee Valgus/Varus Moment

Knee Rotation Moment

Ankle Dors/Plan Moment

Ankle Eversion/Inversion Moment

Ankle Rotation Moment

Total Hip Power

Total Knee Power

Ankle Power

Adult Normal Subjects Information

Temporal Stride Parameters:
Walking Speed (m/s): Avg- 1.155 , SD- 0.142
Stride Length (m): Avg- 1.295 , SD- 0.098
Cadence (step/min)- Avg- 53.548 , SD- 5.842

Male: 5 , Female: 3
Left: 7 , Right: 7
Height (m): Avg- 1.73 , SD- 0.075
Weight (kg): Avg- 72.1 , SD- 12.887
Age: Avg- 22 , SD- 1.323

B.4   Subject 2 Normal Ambulation Gait Report
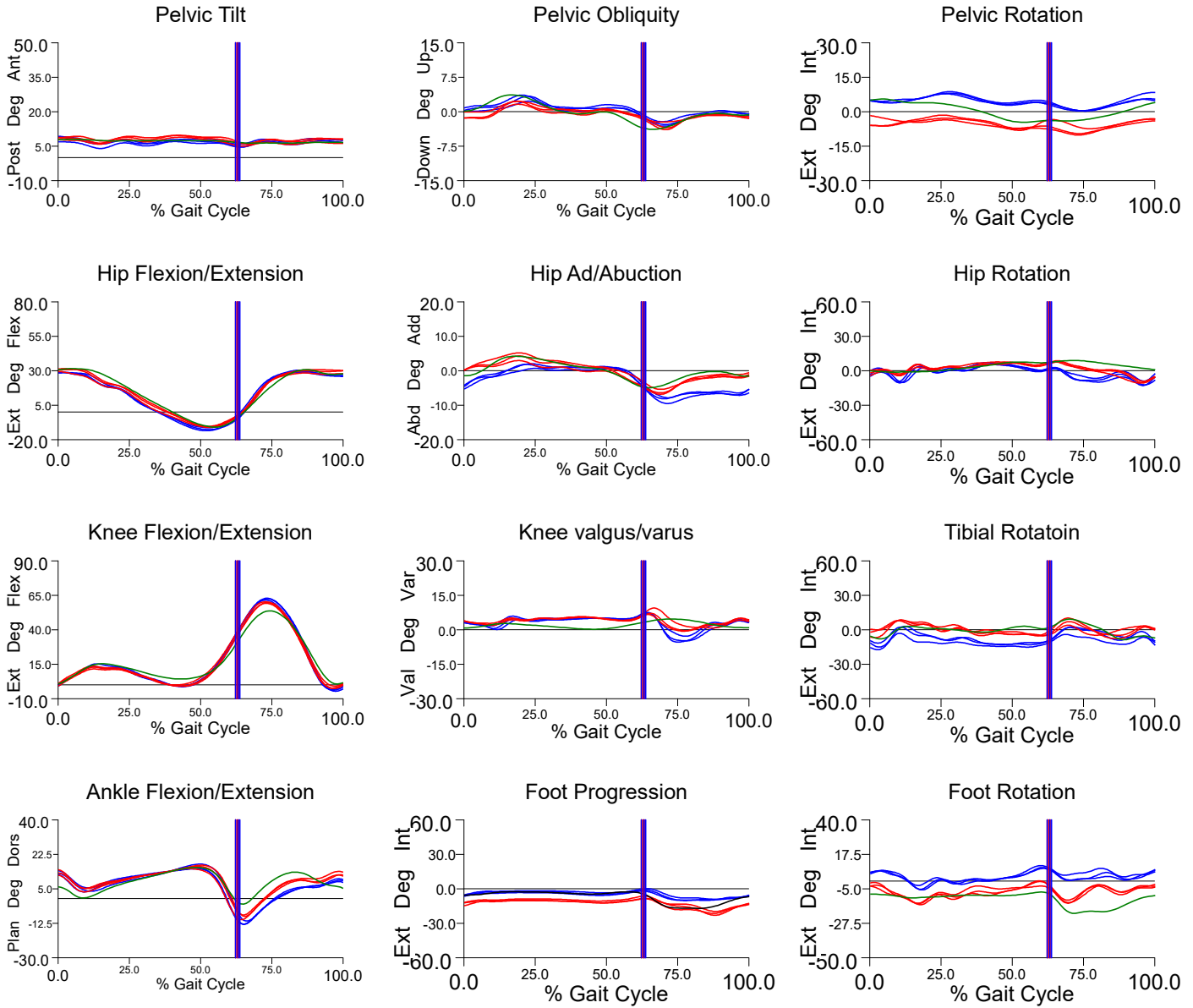
Kinematics and Temporal Parameters

Pelvic Tilt	Pelvic Obliquity	Pelvic Rotation

Speed	1.25 m/s	0.70 Statures/s
Stride	Wid : NO_DATA (0)	Len(6) 1.42±0.03m
Cycle Time	Computed: 1.14 s	Actual (6) 1.14±0.04 s

	Measure±StdDev (Count)	Measure±StdDev (Count)
Stance Time	Left : 0.72±0.03 s (3)	Right : 0.71±0.01 s (3)
Swing Time	Left : 0.43±0.02 s (3)	Right : 0.42±0.01 s (3)
Cycle Time	Left : 1.15±0.05 s (3)	Right : 1.13±0.01 s (3)
Strides / Minute	Left : 52.37±2.44 (3)	Right : 53.34±0.40 (3)

Dbl Limb Support (0)   **NO_DATA**
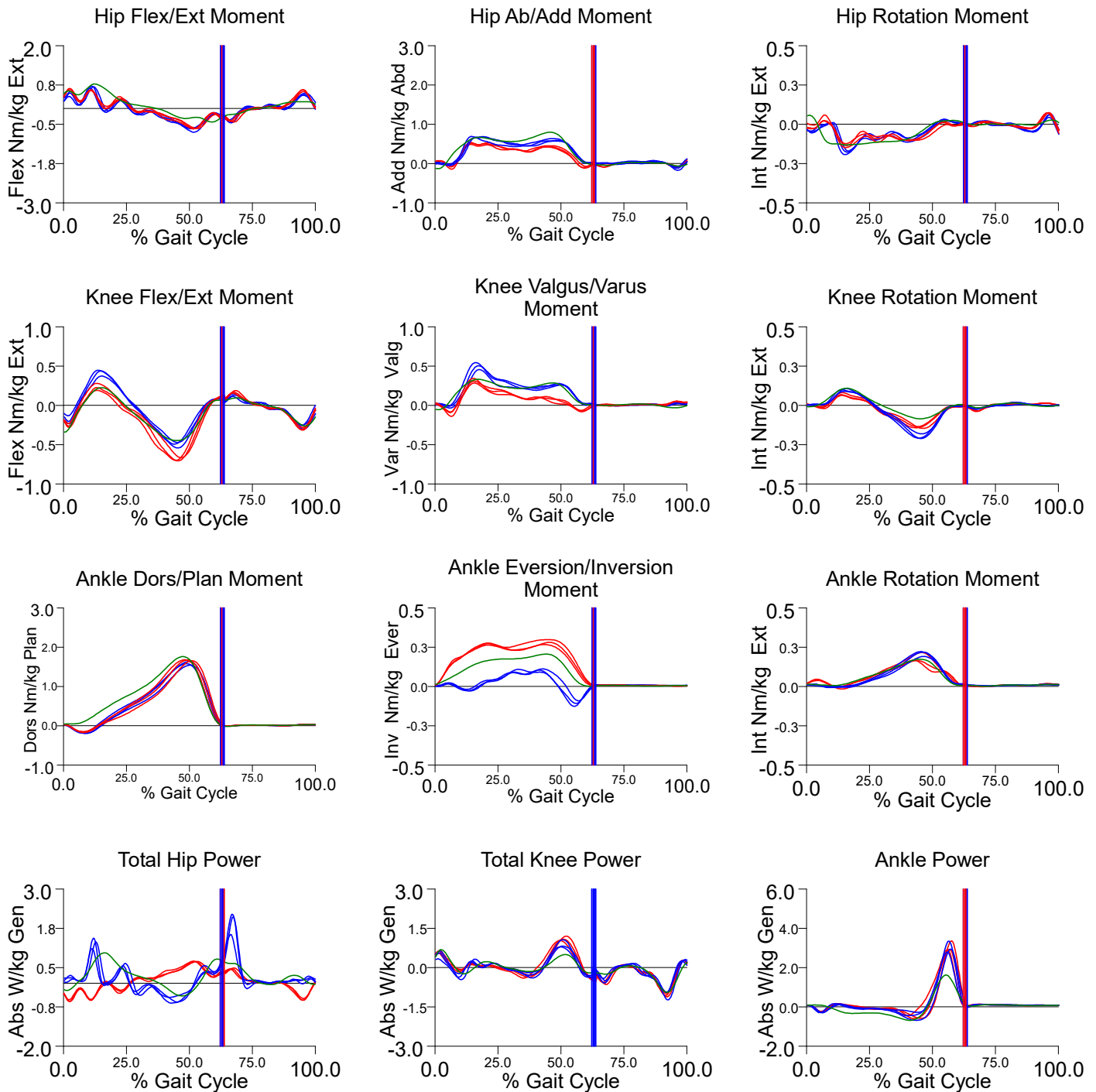
Kinetic Parameters

Hip Flex/Ext Moment · Hip Ab/Add Moment · Hip Rotation Moment · Knee Flex/Ext Moment · Knee Valgus/Varus Moment · Knee Rotation Moment · Ankle Dors/Plan Moment · Ankle Eversion/Inversion Moment · Ankle Rotation Moment · Total Hip Power · Total Knee Power · Ankle Power

Adult Normal Subjects Information

Temporal Stride Parameters:
Walking Speed (m/s): Avg- 1.155 , SD- 0.142
Stride Length (m): Avg- 1.295 , SD- 0.098
Cadence (step/min)- Avg- 53.548 , SD- 5.842

Male: 5 , Female: 3
Left: 7 , Right: 7
Height (m): Avg- 1.73 , SD- 0.075
Weight (kg): Avg- 72.1 , SD- 12.887
Age: Avg- 22 , SD- 1.323

B.5   Subject 2 Rigid-Ankle Ambulation Gait Report
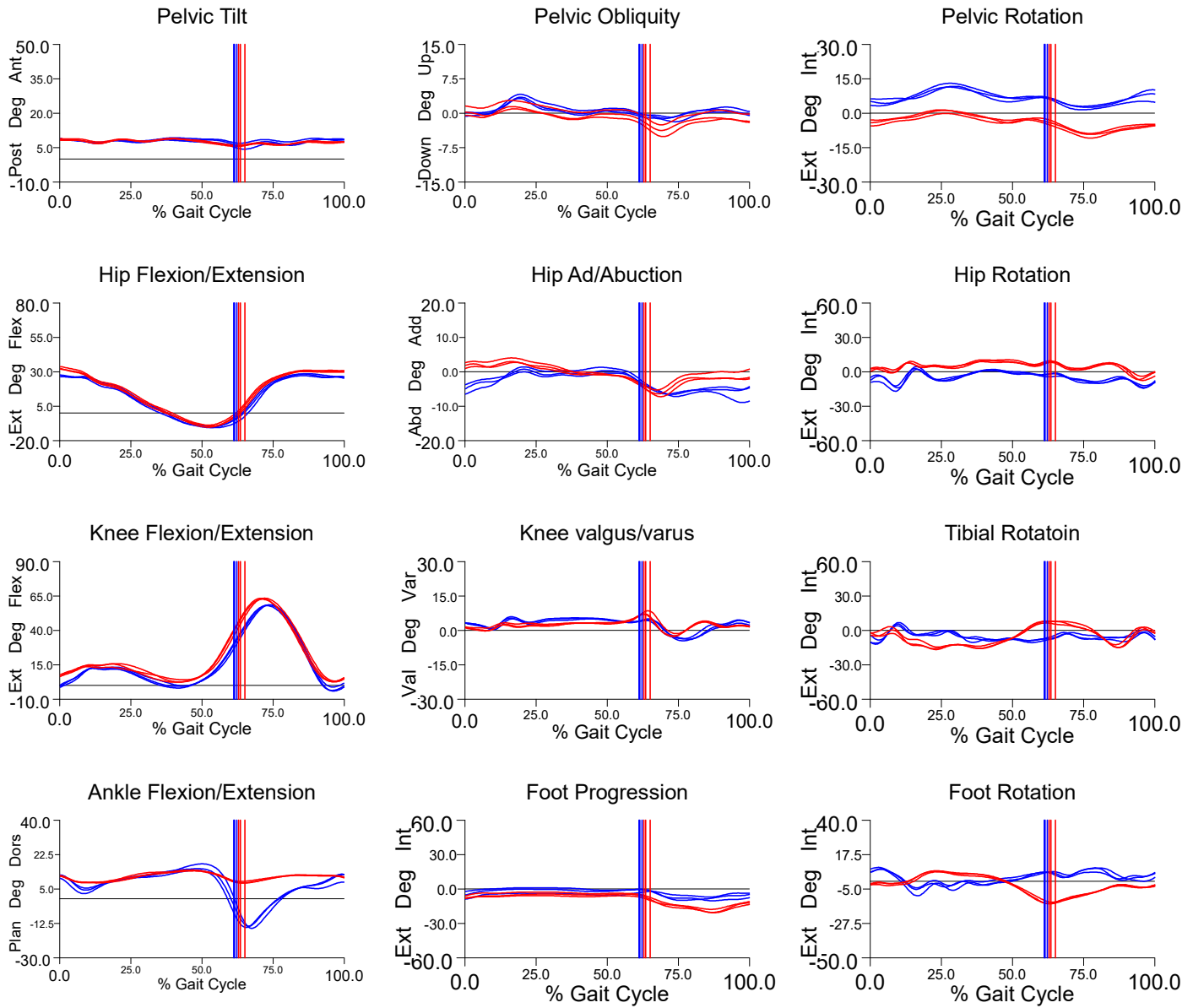
Kinematics and Temporal Parameters

Pelvic Tilt
Pelvic Obliquity
Pelvic Rotation
Hip Flexion/Extension
Hip Ad/Abuction
Hip Rotation
Knee Flexion/Extension
Knee valgus/varus
Tibial Rotatoin
Ankle Flexion/Extension
Foot Progression
Foot Rotation

Speed	1.12 m/s		0.63 Statures/s	
Stride	Wid : NO_DATA (0)		Len(6) 1.33±0.02m	
Cycle Time	Computed: 1.19 s		Actual (6) 1.19±0.02 s	
	Measure±StdDev (Count)		Measure±StdDev (Count)	
Stance Time	Left : 0.76±0.01 s (4)		Right : 0.73±0.02 s (3)	
Swing Time	Left : 0.43±0.02 s (3)		Right : 0.45±0.00 s (3)	
Cycle Time	Left : 1.20±0.01 s (3)		Right : 1.18±0.02 s (3)	
Strides / Minute	Left : 50.06±0.61 (3)		Right : 50.65±0.74 (3)	

Dbl Limb Support (0) **NO_DATA**

Kinetic Parameters

Hip Flex/Ext Moment

Hip Ab/Add Moment

Hip Rotation Moment

Knee Flex/Ext Moment

Knee Valgus/Varus Moment

Knee Rotation Moment

Ankle Dors/Plan Moment

Ankle Eversion/Inversion Moment

Ankle Rotation Moment

Total Hip Power

Total Knee Power

Ankle Power

Adult Normal Subjects Information

Temporal Stride Parameters:
Walking Speed (m/s): Avg- 1.155 , SD- 0.142
Stride Length (m): Avg- 1.295 , SD- 0.098
Cadence (step/min)- Avg- 53.548 , SD- 5.842

Male: 5 , Female: 3
Left: 7 , Right: 7
Height (m): Avg- 1.73 , SD- 0.075
Weight (kg): Avg- 72.1 , SD- 12.887
Age: Avg- 22 , SD- 1.323